

Figure credit: Cover art was created by: Bonfá, ALO; Alves, ED; Fabrício, V; Nonaka, KO; Anselmo-Franci, JA; Achcar, JA; Montrezor, LH. Cover design: Matheus Celestino



# Simultaneous alterations in ovaries and bone as a result of polycystic ovary syndrome

Bonfá, ALO.<sup>1</sup>; Alves, ED<sup>1</sup>; Fabrício, V<sup>2,3</sup>; Nonaka, KO<sup>3</sup>; Anselmo-Franci, JA<sup>4</sup>; Achcar, JA<sup>1</sup>; Montrezor, LH<sup>1\*</sup>

\*Corresponding author: E-mail address: [lhmontrezor@uniara.edu.br](mailto:lhmontrezor@uniara.edu.br)

**Abstract:** Polycystic ovary syndrome (PCOS) is one of the most widely recognized endocrine disorders affecting reproductive-age women. The etiopathogenesis and mechanisms of this syndrome remain unclear. Diagnosis requires two of the following: polycystic ovaries, oligo- or anovulation, and hyperandrogenism. Most women with PCOS display conditions such as metabolic abnormalities, diabetes, obesity, cardiovascular disease, and/or bone dysfunction. Considering the ethical limitations of human studies, animal and cell culture models that reflect some features of PCOS are important for investigation of this syndrome. The aim of the present work was to study some of the endocrine relationships between ovaries and bone tissue in a polycystic ovary syndrome animal model. The study was performed using an estradiol valerate PCOS-induced rat model (n = 30) and bone mesenchymal stem cell cultured from bone marrow of those animals. It was hypothesized that changes of the endocrine relationship between ovaries and bones could be observed in from in vivo animal model and in vitro cell culture assays. The ovarian morphological and endocrine changes seem to be correlated with endocrine, biophysical, and biomechanical changes in bone properties. Mesenchymal stem cells obtained from PCOS-induced rats, cultured for up to 21 days and differentiated into osteoblasts, presented lower viability and reduced mineralization of the extracellular matrix. Taken together, these results indicate important endocrine and structural effects of PCOS in ovaries and bones, contributing to part of the understanding of the pathophysiological mechanisms of PCOS.

**Keywords:** Polycystic Ovary Syndrome. Animal Model. Cell Culture. Bone. Osteocalcin.

## Introduction

Polycystic ovary syndrome (PCOS) is one of the commonest endocrine disorders in women of reproductive age, with worldwide prevalence from 2% to 27%, depending on the diagnostic criteria used<sup>1-6</sup>. Diagnosis of PCOS based on the Rotterdam Consensus criteria requires two of the following: polycystic ovaries, hyperandrogenism, and oligomenorrhea or amenorrhea. This reproductive endocrinopathy is associated with hyperandrogenism, hirsutism, polycystic or polyfollicular ovaries, oligo/anovulation, infertility, luteinizing hormone (LH) hypersecretion, increased levels of inflammatory markers, obesity, dyslipidemia, insulin resistance (IR), type 2 diabetes, metabolic syndrome, and bone abnormalities<sup>5,7-16</sup>.

Androgen excess is a complex reproductive disorder also associated with IR, obesity, hyperlipidemia, hypertension, endothelial dysfunctions, and bone dysfunctions<sup>17-20</sup>. Androgen insufficiency and androgen excess both cause ovarian dysfunction. Lack of androgen in the ovary, specifically in granulosa cells, leads to ovarian insufficiency, while excess androgen is linked to PCOS. Excess androgen appears to be both a cause and a consequence of PCOS, in a vicious cycle<sup>21</sup>. Androgen receptors (AR) are expressed in all the bone cells, including osteoblasts, osteoclasts, and osteocytes<sup>22</sup>, indicating the direct influence of androgen on bone. Bone mineral density (BMD) is higher in PCOS amenorrheic women than in non-PCOS amenorrheic women, while hyperandrogenic women with regular menses have been shown to have significantly higher BMD than either amenorrheic hyperandrogenic women or controls<sup>23</sup>. The excess of androgen in PCOS subjects affects the bone mass directly, as well as by the involvement of various other factors, such as insulin, glucose, and cytokines<sup>19</sup>.

Assessment of the etiology of PCOS and evaluation of the long-term risks of PCOS, in relation to bone development and metabolic and reproductive diseases, requires the development of suitable animal models<sup>24</sup>. Information is limited concerning methods for establishing animal models of PCOS, although several animal models have been developed and studied for the human PCOS<sup>24-29</sup>. However, the etiology of PCOS is still unclear, due to its complex manifestation as a syndrome and the limitations of translational studies using animals.

In order to understand some of the endocrine relationships between ovaries and bone tissue in a polycystic ovary syndrome situation, an animal model with PCOS induced with estradiol valerate was used, considering a period of 60 days post-induction. In addition, bone mesenchymal stem cells were cultured for up to 21 days, with differentiation into osteoblasts, in order to evaluate whether endocrine effects *in vivo* could compromise cell viability and mineralization of the extracellular matrix.

## MATERIAL AND METHODS IN VIVO EXPERIMENTS

### Animals

Thirty adult female Wistar rats (6-months old at the end of the experiments) were used. The animals were weighed at the beginning of the experiment (204.2 ± 11.04 g), housed in standard boxes (n = 5), and kept at the University of Araraquara (UNIARA, Araraquara, São Paulo State, Brazil), under controlled conditions of 22 ± 2 °C and 12-h light/dark cycles (lights on at 7:00 a.m.). Water and feed were offered *ad libitum*. All the experimental procedures were approved by the Committee of Ethics in Animal Use (CEUA/UNIARA protocol n°

<sup>1</sup> Department of Biological Science and Health – Biotechnology, University of Araraquara – UNIARA, Araraquara, SP, Brazil.

<sup>2</sup> Department Health Science, University Oeste Paulista – UNOESTE, Jaú, SP, Brazil

<sup>3</sup> Biological Sciences and Health Center – UFSCar, São Carlos, SP, Brazil.

<sup>4</sup> Department of Morphology, Physiology and Basic Pathology – USP, Ribeirão Preto, SP, Brazil.

018/2016), following the norms of the National Council for Control of Animal Experimentation (CONCEA/MCTI, Brazil).

### ***Estrous cycle, body mass and induction of polycystic ovary***

Estrous cycle analysis was performed daily for 4 weeks prior to induction of PCOS, in order to confirm the occurrence of normal and consecutive cycles. The rats that were used in the experiment had at least 4 normal and consecutive cycles<sup>30-31</sup>. The estrous cycle checks were continued daily until the end of the experimental periods.

Body mass analysis of the rats was performed on the day of arrival at the laboratory, on the day of induction of PCOS, weekly after the day of induction, and on the days of euthanasia.

The polycystic ovary induction was performed with a single dose of estradiol valerate (EV) (Sigma–Aldrich, MO, USA) dissolved in mineral oil (2.0 mg/0.2 mL/rat; intramuscular)<sup>30</sup>. Control (C) animals received intramuscular injection of 0.2 mL of mineral oil. After hormonal and mineral oil injections, the animals were divided into 6 groups (n = 5) that were evaluated after different periods: 30 days after induction (PCO 30 and C 30 groups), 45 days after induction (PCO 45 and C 45 groups), and 60 days after induction (PCO 60 and C 60 groups). The evaluation times were based on the time required for PCOS to appear<sup>30-32</sup>. The PCOS–induced rats showed important signs related to the syndrome, including hyperandrogenemia, irregular estrous cycles, and polycystic ovarian morphology.

### ***Progesterone, testosterone, luteinizing hormone, alkaline phosphatase, and osteocalcin assays***

Immediately after euthanasia, blood was collected by cardiac puncture and/or aortic arch, using heparinized syringes. The blood was centrifuged at 3000 rpm for 20 minutes to obtain the plasma, which was transferred to Eppendorf tubes and frozen at –20 °C for subsequent analyses of progesterone (P4), testosterone (T), luteinizing hormone, alkaline phosphatase (ALP), and osteocalcin (OCN). The plasma progesterone and testosterone concentrations were determined by double–antibody radioimmunoassay (RIA), using MAIA kits provided by Biochemistry Immunosystem (Bologna, Italy). The lower limits of detection for progesterone and testosterone were 0.02 ng/mL and 5.0 pg/mL, respectively. The intra–assay coefficients of variation were 7.5% for progesterone and 4% for testosterone. Plasma LH was assayed using specific kits provided by the National Hormone and Peptide Program (Harbor–UCLA, USA). The antiserum for LH was LH–S10, using RP3 as reference. The lower limit of detection was 0.04 ng/mL and the intra–assay coefficient of variation was 3.4%. Alkaline phosphatase activity was determined from measurements of the release of thymolphthalein from thymolphthalein monophosphate, using a commercial kit (Labtest Diagnóstica, Belo Horizonte, MG, Brazil). Aliquots of 50 µL of the culture medium were used. The absorbance was measured at 590 nm and the ALP activity was calculated based on the value for a standard. Osteocalcin was analyzed by electrochemiluminescence immunoassay, using a COBAS 6000 immunoassay analyzer (Roche Diagnostic, Germany). The inter–assay coefficient of variation was 4.8%.

### ***Gonadosomatic index and bone biomechanical parameters***

The animals were weighed before euthanasia. Subsequently, the ovaries were removed, cleaned, and weighed. The values obtained were used to determine the gonadosomatic index (GSI), as follows: (ovarian mass/body mass) x 100.

Immediately after euthanasia, the femoral bones were removed and dissected to remove the muscle and soft tissue. The isolated bone material was maintained in 0.9% saline solution, at –20 °C, for subsequent analysis. The right femurs were removed and cleaned for determination of BMD and bone mineral content (BMC), according to the Archimedes Principle<sup>33</sup>. The biomechanical parameters of the right femurs were obtained by the three–point bending test, using a universal test machine (Model 4444, INSTRON) and a load cell with maximum capacity of 100 kgf, at a speed of 5 mm/min<sup>34</sup>. The test results were recorded in graphical form using Instron Series IX software, generating load versus displacement curves. Analysis of the curve provided the following parameters: maximum load, maximum load at fracture, and stiffness.

### ***Ex Vivo Experiments***

#### ***Mesenchymal stem cells***

Mesenchymal stem cells were obtained from the left femurs of the control and PCOS females (30, 45, and 60 days), with isolation according to the Wang protocol<sup>35</sup>. Briefly, after euthanasia, the femurs were removed from the animals, dissected, and transferred to Falcon tubes containing DMEM (Dulbecco's Modified Eagle Medium) supplemented with NaHCO<sub>3</sub>, L–glutamine, 10% fetal bovine serum, penicillin (100 U/mL), and streptomycin (100 µg/mL). Under aseptic conditions, the femur proximal and distal epiphyses were sectioned with surgical pliers. The cells were extracted by flushing the bone marrow using a syringe (20 mL) and needle (25 x 8). The cell suspension obtained was centrifuged (10000 rpm for 4 minutes at 4 °C), the supernatant was discarded, and the cells were resuspended in culture medium. The cell pools (for each experimental time: 30, 45, and 60 days) were prepared in culture bottles, with one pool obtained

from the control animals and another from the PCOS animals. The culture bottles were kept under controlled conditions (37 °C, 5% CO<sub>2</sub>, and 95% atmospheric air), until the cells reached 70–80% confluence (approximately 10 days). The culture medium was changed every 48 h.

### **Mesenchymal stem cell differentiation**

After reaching cell confluency in the bottles, the cells were transferred to 24-well culture plates, at a density of 3 x 10<sup>4</sup> cells/mL/well, with osteogenic differentiation medium<sup>36</sup> (ascorbic acid, dexamethasone, and β-glycerophosphate – Sigma–Aldrich, St. Louis, MO, USA) added to the control medium (DMEM). The culture plates for the control and the PCOS groups (for each experimental time: 30, 45, and 60 days) were kept (in triplicate for each experimental time) under conditions of 37 °C, 5% CO<sub>2</sub>, and 95% atmospheric air for 7, 14, and 21 days after addition of the osteogenic medium. The culture medium was changed every 72 h and it was frozen at –20 °C for subsequent analysis of alkaline phosphatase.

### **Cell metabolic activity**

Cell metabolic activity was assessed after 7, 14, and 21 days of culture, using the colorimetric assay involving the reduction of 3- (4,5-dimethylthiazol-2-yl)-2,5- diphenyltetrazolium bromide (MTT) (Sigma–Aldrich, St. Louis, MO, USA), with formation of formazan (a blue crystalline product), by the action of mitochondrial dehydrogenase in viable cells. The quantity of the product is directly proportional to the blue coloration, enabling estimation of the number of mitochondria and, consequently, the number of viable cells in the culture, hence providing an indirect measure of cell metabolic activity. After removal of the culture medium from the wells, 50 μL of MTT (0.5 mg/mL) was added to each well and the plate was incubated for 4 h at 37 °C, under 5% CO<sub>2</sub>. Subsequently, 100 μL of acid isopropanol was added to each well, in order to fully solubilize the precipitate formed, and the absorbance of the solution was measured at 570 nm<sup>37</sup>, using a microplate reader (Polaris, Celer Biotecnologia, Belo Horizonte, MG, Brazil).

### **Mineralization nodes analysis**

The method described by Gregory et al.<sup>38</sup> was used to detect extracellular matrix mineralization. Briefly, after 7, 14, and 21 days of culture, the plate wells containing osteogenic cells were washed with cold phosphate–buffered saline (PBS) (Sigma–Aldrich, St. Louis, MO, USA), filled with formaldehyde (10% v/v) (Merck, Kenilworth, NJ, USA), and left for 30 min. The wells were then washed with deionized water, followed by addition of 1 mL of Alizarin Red solution (Sigma–Aldrich, St. Louis, MO, USA). After 30 min, the excess Alizarin Red solution was removed, the wells were washed with water, and the plates were kept at room temperature for the wells to dry. Quantification of extracellular matrix mineralization was performed by adding 450 μL of acetic acid solution (10% v/v) to each well that had been previously stained with Alizarin Red. The plates were kept on a shaker for 30 min, at room temperature, after which 400 μL aliquots of the contents of the wells were transferred to Eppendorf tubes, followed by addition of 150 μL of ammonium hydroxide (NH<sub>4</sub>OH). Finally, the contents of the Eppendorf tubes were transferred to 96-well plates and the absorbances were measured at 405 nm with a microplate reader.

### **Statistical analysis**

The results are reported as mean ± SEM. The data were analyzed using ANOVA (analysis of variance), with one classification for six independent groups of measures, and a Fisher test was used for multiple comparisons. The statistical analyses were performed with SigmaStat software (Systat Software, Point Richmond, CA, USA). Statistically significant differences among the means for the treatment groups considered a p-values < 0.05. Logarithmic data transformation was used to satisfy the assumptions of the ANOVA model (normality and constant variance of the errors). These assumptions were confirmed using residual plots.

## **Results**

### **in vivo experiments**

#### **Body mass, ovary mass, and GSI**

There were no significant differences of body mass between the control and PCO animals (Figs. 1A, 1C, and 1E). For the 30-day groups (Fig. 1B), the left ovary mass was higher for the control animals (0.0727 ± 0.0228 g), compared to the PCO animals (0.0454 ± 0.0158 g). For the 45-day groups (Fig. 1D), the right ovary mass was lower for the PCO group (0.0346 ± 0.0054 g), compared to the control group (0.054 ± 0.012 g). For the 60-day groups (Fig. 1F), the masses of both ovaries were higher for the PCO group (right: 0.0552 ± 0.0059 g; left: 0.0554 ± 0.0035 g), compared to the control group (right: 0.0482 ± 0.002 g; left: 0.046 ± 0.0051 g).

Table 1 presents the gonadosomatic index results. The GSI values for the 30-day PCO groups (0.023 ± 0.0015)

and the 45-day PCO group ( $0.014 \pm 0.0006$ ) were lower than for the corresponding control groups (30 days:  $0.029 \pm 0.0021$ ; 45 days:  $0.021 \pm 0.0015$ ). For the 60-day groups, the GSI was higher for the PCO group ( $0.024 \pm 0.0016$ ), compared to the control group ( $0.019 \pm 0.0009$ ). An effect of time on GSI was also observed. For the control groups, GSI was higher for the 30-day group, with 60-day group presenting the lowest GSI. Among the PCO groups, the lowest GSI was observed for the 45-day group.

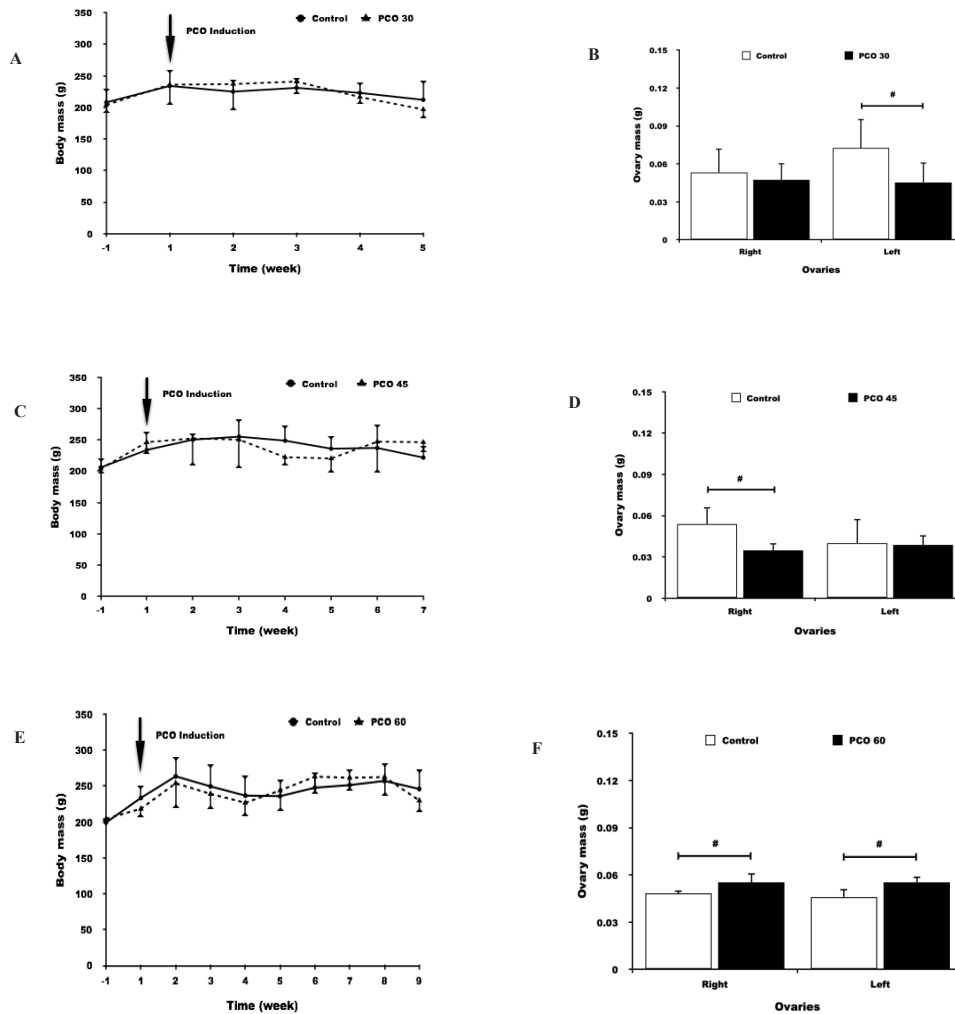


**Figure 1.** Mean biometric data variations for the control and PCO rats. 30-day groups: body mass (A), and ovary mass (B); 45-day groups: body mass (C), and ovary mass (D); 60-day groups: body mass (E), and ovary mass (F). The data are shown as mean  $\pm$  SEM ( $n = 5$ ). # Significant difference ( $p$ -values  $< 0.05$ ).

**Table 1.** Gonadosomatic index (GSI), alkaline phosphatase (ALP), progesterone (P4), testosterone (T), luteinizing hormone (LH), and osteocalcin (OCN) values for the control and PCO groups (30, 45, and 60 days) of female adult rats. The data are shown as mean  $\pm$  SEM ( $n = 5$  per group). Different superscript lower case letters indicate significant differences ( $p$ -values  $< 0.05$ ).

	Control			PCO		
	30 days	45 days	60 days	30 days	45 days	60 days
GSI (%)	$0.029 \pm 0.002^a$	$0.0021 \pm 0.0015^b$	$0.019 \pm 0.0009^c$	$0.023 \pm 0.0015^b$	$0.014 \pm 0.006^c$	$0.024 \pm 0.0016^b$
ALP (IU/L)	$60 \pm 18.31^b$	$81.11 \pm 23.58^b$	$70.66 \pm 29.52^b$	$139.74 \pm 27.09^a$	$114 \pm 28.04^a$	$107.45 \pm 20.97^a$
P4 (ng/mL)	$38.22 \pm 28.53$	$17.27 \pm 8.768$	$26.16 \pm 14.21$	$4.154 \pm 4.549$	$17.98 \pm 14.74$	$23.13 \pm 21.33$
T (pg/mL)	$6.732 \pm 2.5788^b$	$28.23 \pm 16.51^a$	$24.51 \pm 7.26^a$	$23.86 \pm 11.028^a$	$19.81 \pm 9.47^a$	$48.79 \pm 30.28^a$
LH (ng/mL)	$0.806 \pm 0.376^a$	$1.146 \pm 1.036^a$	$0.5652 \pm 0.1825^a$	$1.137 \pm 0.842^a$	$0.2116 \pm 0.1025^b$	$0.638 \pm 0.508^{ab}$
OCN (ng/mL)	$21 \pm 2.13^a$	$19.25 \pm 1.31^a$	$17.5 \pm 2.01^a$	$14.25 \pm 1.01^b$	$17 \pm 1.98^{ab}$	$14.5 \pm 1.2^b$

**Femurs biomechanical parameters**

For the 60-day groups, the maximum load was higher for the control group ( $0.2312 \pm 0.0039$  kN), compared to the PCO group ( $0.1886 \pm 0.0326$  kN). The maximum load showed time dependent effect and was higher for the 60-day group, compared to the 30-day group ( $0.1827 \pm 0.013$  kN) and the 45-day group ( $0.1943 \pm 0.0142$  kN) (Fig. 2A). At 60 days, the maximum load at the fracture point was higher for the control group ( $0.2152 \pm 0.0439$  kN) than for the PCO group ( $0.1147 \pm 0.0588$  kN). For both groups, the maximum load at the fracture point was time dependent.

In the case of the control groups, a higher value was obtained for the 60-day group ( $0.2152 \pm 0.0439$  kN), compared to the 30-day group ( $0.1579 \pm 0.016$  kN) and the 45-day group ( $0.177 \pm 0.0193$  kN). The value for the 60-day PCO group ( $0.1147 \pm 0.0588$  kN) was lower than for the 30-day PCO group ( $0.1707 \pm 0.037$  kN) and the PCO 45-day group ( $0.1754 \pm 0.0297$  kN) (Fig. 2C).

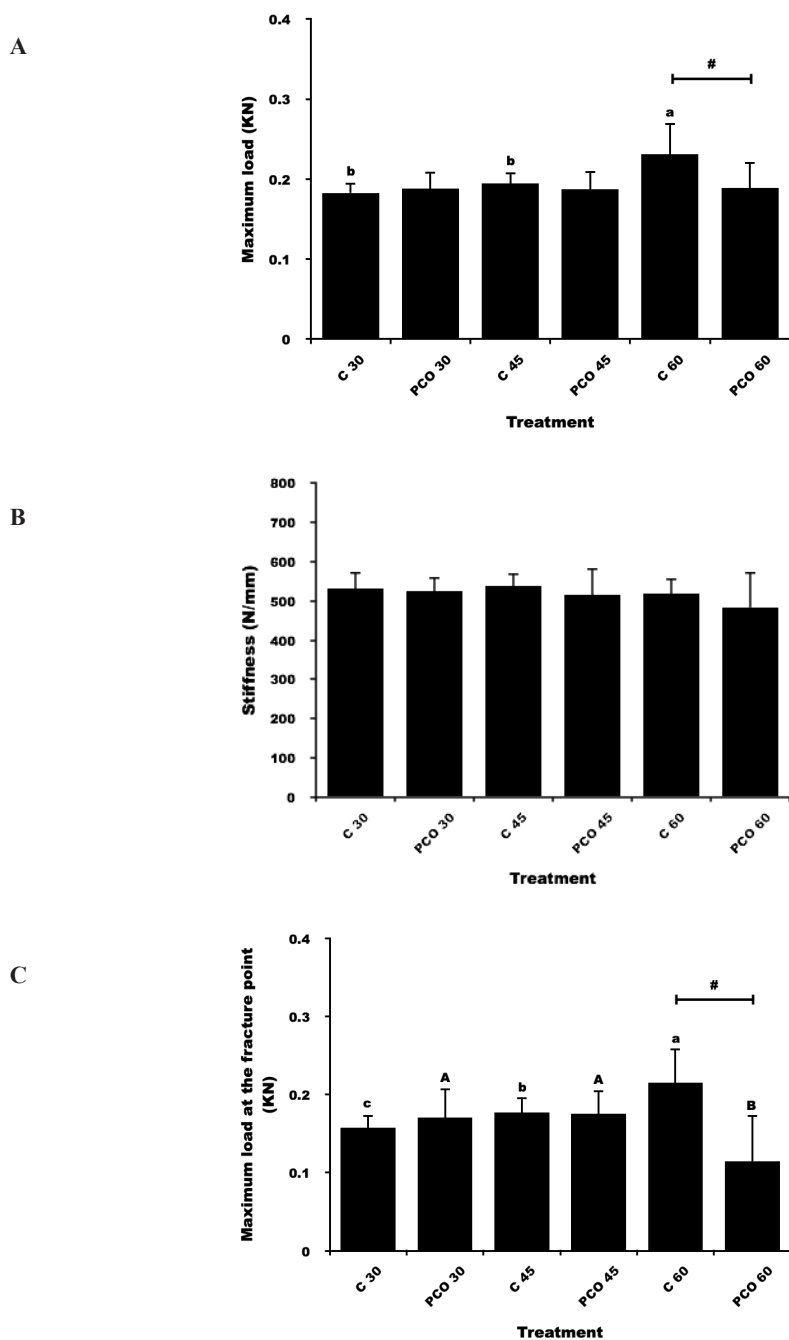


**Figure 2.** Biomechanical parameters for the femurs of the rats in the control (C 30, C 45, and C 60), and polycystic ovary (PCO 30, PCO 45, and PCO 60) groups: (A) maximum load; (B) stiffness; (C) maximum load at the fracture point. The data are shown as mean ± SEM (n = 5). Different lower case letters indicate differences between the control groups. Different capital letters indicate differences between the PCO groups. # Difference between the control and PCO rats (p-values < 0.05).

**Plasma levels of alkaline phosphatase and osteocalcin**

Increases in plasma alkaline phosphatase concentrations (Table 1) were observed for all the PCO groups (30-day:  $139.74 \pm 27.09$  IU/L; 45-day:  $114 \pm 28.04$  IU/L; and 60-day:  $107.45 \pm 20.97$  IU/L), compared to the corresponding control groups (30-day:  $60 \pm 18.31$  IU/L; 45-day:  $81.11 \pm 23.58$  IU/L; 60-day:  $70.66 \pm 29.52$  IU/L).

The plasma osteocalcin concentration (Table 1) was lower for the 30-day PCO group ( $14.25 \pm 1.01$  ng/mL), compared to the 30-day control group ( $21 \pm 2.13$  ng/mL). The 60-day PCO group presented a lower osteocalcin concentration ( $14.5 \pm 1.2$  ng/mL) than the 60-day control group ( $17.5 \pm 2.01$  ng/mL).

**Plasma progesterone, testosterone, and luteinizing hormone concentrations**

The variations of progesterone, testosterone, and luteinizing hormone are shown in Table 1. There were no significant differences in plasma progesterone concentrations, despite important biological variations of the P4. Lower plasma T concentration was observed for the 30-day control group ( $6.732 \pm 2.578$  pg/mL), compared to the other groups. Significantly lower plasma LH was found for the 45-day PCO group ( $0.2116 \pm 0.1025$  ng/mL), compared to the other experimental groups, with the exception of the 60-day PCO group ( $0.638 \pm 0.508$  ng/mL).

**IN VITRO EXPERIMENTS**

**Cellular metabolic activity**

The 30-day PCO group showed lower cellular metabolic activity, compared to the 30-day control group, for all culture times: 7 days (C:  $0.2423 \pm 0.008$ ; PCO:  $0.166 \pm 0.007$ ), 14 days (C:  $0.2413 \pm 0.009$ ; PCO:  $0.1586 \pm 0.006$ ), and 21 days (C:  $0.2870 \pm 0.01$ ; PCO:  $0.1473 \pm 0.016$ ). Among the control groups, the highest cellular metabolic activity was observed with 21 days of culture ( $0.2870 \pm 0.01$ ) (Fig. 3A).

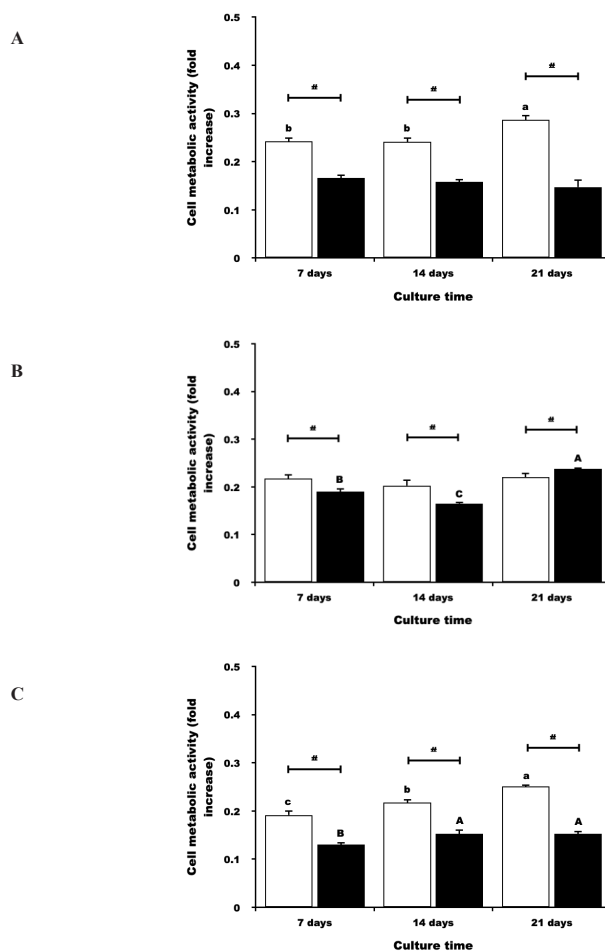


**Figure 3.** Cellular metabolic activity determined by reduction of methylthiazolyl-diphenyl-tetrazolium bromide (MTT), with absorbance at a wavelength of 570 nm. Cells were cultured for 7, 14, and 21 days. (A) 30-day groups, (B) 45-day groups, and (C) 60-day groups. The white and black columns correspond to the control and PCO groups, respectively. The data are shown as mean  $\pm$  SEM (n = 5). Different lower case letters indicate differences between control groups. Different capital letters indicate differences between PCO groups. # Difference between control and PCO rats (p-values < 0.05).

The cellular metabolic activity of the 45-day PCO group was lower than that of the control group for culture time of 7 days (C:  $0.2173 \pm 0.009$ ; PCO:  $0.19 \pm 0.007$ ) and 14 days (C:  $0.2026 \pm 0.013$ ; PCO:  $0.165 \pm 0.004$ ). For the culture time of 21 days, the 45-day PCO group presented higher metabolic activity ( $0.2376 \pm 0.006$ ) than the 45-day control group ( $0.2206 \pm 0.009$ ). Among the PCO groups, the highest metabolic activity was observed with 21 days of culture ( $0.2376 \pm 0.006$ ) (Fig. 3B).

The cellular metabolic activity of the 60-day PCO group was lower than that of the control group, for all the culture times analyzed: 7 days (C:  $0.1916 \pm 0.01$ ; PCO:  $0.1303 \pm 0.005$ ), 14 days (C:  $0.2176 \pm 0.007$ ; PCO:  $0.1526 \pm 0.009$ ), and 21 days (C:  $0.2513 \pm 0.004$ ; PCO:  $0.1530 \pm 0.006$ ) (Fig. 3C). Among the 60-day control groups, the highest cellular metabolic activity was observed with culturing for 21 days ( $0.2513 \pm 0.004$ ). Among the 60-day PCO groups, the highest cellular metabolic activities were observed with culturing for 14 days ( $0.1526 \pm 0.009$ ) and 21 days ( $0.1530 \pm 0.006$ ) (Fig. 3C).

### Organic mineralization

When the mesenchymal stem cells were differentiated into osteoblasts kept in culture for 21 days, the 30-day control group showed higher mineralization at 14 days of culture ( $3.27 \pm 0.114$ ) and lower mineralization at 21 days of culture ( $0.233 \pm 0.0294$ ). Similar results were observed for the 30-day PCO group, with higher mineralization at 14 days of culture ( $3.1193 \pm 0.1156$ ) and lower mineralization at 21 days ( $0.218 \pm 0.0234$ ) (Fig. 4A).

The organic mineralization of the 45-day groups is shown in Fig. 4B. The control group showed the highest mineralization at 14 days of culture ( $0.8038 \pm 0.0647$ ) and the lowest mineralization at 21 days ( $0.2493 \pm 0.0345$ ). The PCO group showed similar behavior, with the highest mineralization at 14 days of culture ( $0.717 \pm 0.0123$ ) and the lowest mineralization at 21 days ( $0.23 \pm 0.0193$ ).

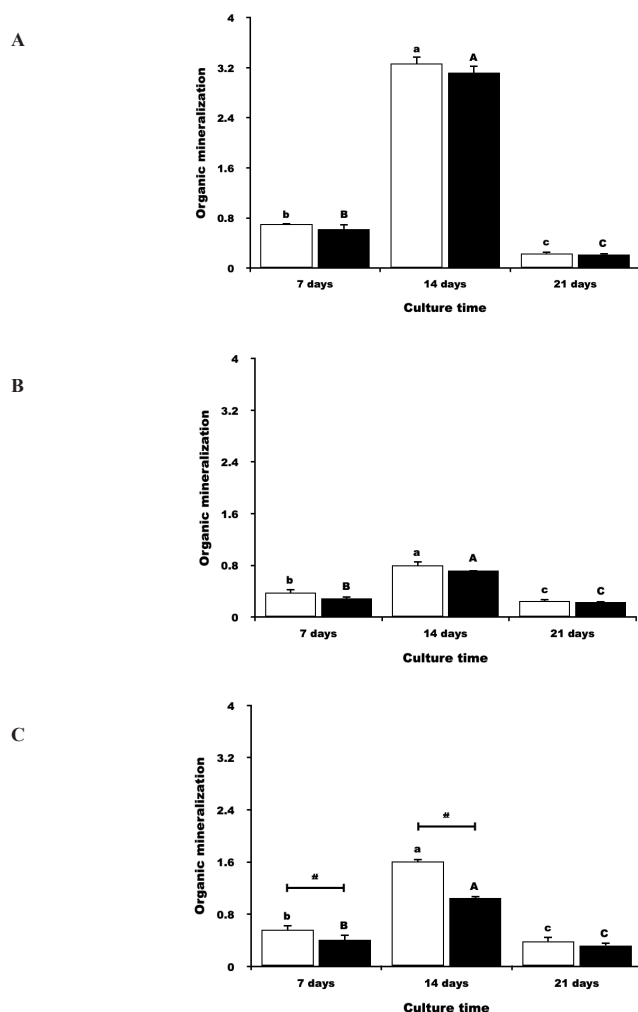


**Figure 4.** Organic mineralization of osteoblasts cultured for 7, 14, and 21 days: (A) 30-day PCO group; (B) 45-day PCO group; (C) 60-day PCO group. The white and black columns correspond to the control and PCO groups, respectively. The data are shown as mean  $\pm$  SEM ( $n = 5$ ). Different lower case letters indicate differences between control groups. Different capital letters indicate differences between PCO groups. # Indicates difference between control and PCO rats ( $p$ -values  $< 0.05$ ).

Fig. 4C shows the results for organic mineralization of the cells of the 60-day groups. The control group showed the highest mineralization at 14 days of culture ( $1.6107 \pm 0.0413$ ) and the lowest mineralization at 21 days of culture ( $0.3855 \pm 0.0696$ ). The PCO group also showed higher mineralization at 14 days of culture ( $1.0512 \pm 0.0329$ ) and lower mineralization at 21 days of culture ( $0.3227 \pm 0.0467$ ). Comparison of the control and PCO groups showed that the PCO group presented lower organic mineralization (7 days:  $0.4108 \pm 0.0769$ ; 14 days:  $1.0512 \pm 0.0329$ ) than the control groups (7 days:  $0.5615 \pm 0.0749$ ; 14-days:  $1.6107 \pm 0.0413$ ).

## Discussion

The results obtained in the present study using a model of adult Wistar rats induced to PCOS with a single dose of EV showed ovarian and estrous cycle changes, bone property modifications *in vivo* and *in vitro*, and alterations of ALP, OCN, and T in the plasma. Other studies have employed PCOS animal models<sup>24,29,39</sup>, with differences among the findings for PCOS rats being due to factors such as hormone type and dosage, route of administration, timing and duration of exposure, phase of the estrous cycle, and animal ages at the time of the study<sup>5</sup>.

Androgens and AR play important roles in normal follicular development and female fertility. Evidence of the involvement of androgens in folliculogenesis has been found using *in vivo* animal models<sup>26,40</sup>. The synthesis of androgens is under the control of luteinizing hormone from the pituitary and depends on ovarian cell steroidogenic acute regulatory protein (STAR), cholesterol side-chain cleavage cytochrome P450 (CYP11A1), 17 $\mu$ -hydroxylase (CYP17), and 3 $\mu$ -hydroxysteroid dehydrogenase (HSD3B)<sup>26,41</sup>.

Women with PCOS have abnormalities in estrogen and androgen metabolism<sup>14,19,23,42</sup>. Hyperandrogenism is a typical feature of PCOS and often manifests as disturbed folliculogenesis, reduced fertility, and adverse effects on oocyte developmental competence<sup>43</sup>. The results obtained in the present work demonstrated that T levels were elevated in the 60-day animals induced to PCOS, compared to the control animals. It has been reported that the hormone effect in the female reproductive system is strongly influenced by the time of exposure<sup>5,10,21,44</sup>. In the present case, the animal model employed had suitable hyperandrogenic characteristics for the duration of the assays performed. In addition to hyperandrogenism, the rats showed important ovarian alterations, such as reduction of ovarian mass 45 days after induction and increase of ovarian mass at 60 days, which could have been due to a greater number of ovarian cysts. No alteration of body weight was observed, although there was a reduction of GSI of the PCOS animals up to 45 days after EV treatment, followed by an increase at 60 days, suggesting morphological and steroidogenic ovarian alterations. At 60 days after PCOS induction, the treated animals showed increases of GSI and production of T. This was suggestive of a vicious cycle, with the endocrine alteration causing ovary morphological alteration, consequently altering hormone synthesis, which could alter T synthesis, and so on.

Follicular atresia is a complex and multifactorial apoptotic process that depends on apoptosis of granulosa cells<sup>43,45-47</sup>. During cyclic recruitment, atresia is promoted by androgens<sup>48-50</sup>. A single dihydrotestosterone (DHT) injection in hypophysectomized immature female rats was often seen to result in decreased ovarian weight, which was associated with the stimulation of follicular atresia and the reduction of healthy follicles of all types<sup>51</sup>. In the present study, all the rats of the PCO groups showed estrous cycle changes, with irregularities such as the maintenance of a phase of the estrous cycle (for example, diestrus) for several weeks. Such alterations, observed using daily vaginal smears, were in agreement with the morphological alterations of the ovaries. All the animals of the PCO groups showed reductions of the numbers of secondary and tertiary follicles, as well as corpora lutea, while there were increases of the numbers of ovarian cysts and atretic follicles (data not shown), similar to our previous observations<sup>15,31</sup>. These results suggested that the ovarian alterations related to the increase in T production, due to possible enzymatic alterations, were the probable cause of the ovarian morphological changes that altered the estrous cycles in the rats induced to PCOS by EV. In PCOS women, the activities of the CYP17 and HSD3B enzymes were found to increase by more than 500% and 1000%, respectively<sup>19,52</sup>. In addition, elevated plasma T levels did not alter the pituitary activity for LH secretion, since the plasma levels of this gonadotrophin were in agreement with the negative feedback performed by T on the pituitary, suggesting that the animal model used did not present alteration of the hypothalamic-pituitary axis.

The bone remodeling cycle begins with alterations of the extracellular matrix due to stimuli that may be mechanical, electrical, hormonal, and magnetic, which are converted into molecular signals and messages (such as nitrous oxide and prostaglandins, changes in electrical charge, and plasma membrane alterations involving calcium release). Normal plasma concentrations of estrogens and androgens have been shown to increase bone mass in men, women, and animals<sup>5,24,53-54</sup>. Androgen exposure enhances osteoblast differentiation and the synthesis of extracellular matrix proteins such as type 1 collagen, osteocalcin, and osteonectin, in addition to stimulating mineralization<sup>19</sup>. Hence, normal concentrations of androgen have an important role in regulating bone matrix production and mineralization. Sawalha and Kovats<sup>55</sup> demonstrated that different androgens can modulate activity in different parts of the bones.

Osteocalcin, which can act in extracellular matrix mineralization, has been used as a serum marker of osteoblastic

bone formation in both clinical and basic research<sup>56</sup>. Higher BMD has been observed in PCOS amenorrheic women than in non-PCOS amenorrheic patients, while hyperandrogenic women with regular menses exhibited significantly higher BMD than controls or hyperandrogenic patients<sup>19,23</sup>. There is conflicting information concerning the actions of OCN in the reproductive system. Osteocalcin can regulate male fertility, while not affecting female reproduction<sup>57-58</sup>. Testosterone was found to be positively correlated with serum osteocalcin, indirectly supporting the participation of serum osteocalcin in sex hormone regulation<sup>59</sup>. The results of the present work revealed changes in bone activity, both in vivo and in vitro. After 60 days following induction to PCOS, there were decreased of the maximum load at the fracture point and the plasma osteocalcin concentration. At the same time, there was the highest plasma concentrations of T. These observations suggested that testosterone plays a crucial role in mediating bone mass and osteocalcin levels in adult rats induced to PCOS by EV. On the other hand, the increase in circulating osteocalcin levels could provide a further stimulus for increase of plasma T, maintaining a vicious cycle between the bone and the ovaries, in this animal model, as suggested in studies indicating the existence of an independent bone-osteocalcin-gonadal axis<sup>60-61</sup>.

Alkaline phosphatase is a marker of bone formation and bone turnover and is used in the evaluation of skeletal status<sup>62-63</sup>. Elevated serum ALP is correlated with low bone mineral density and greater structural damage. Significant associations between ALP and bone mineral density, after controlling for other variables, suggested that ALP might interact with other factors, leading to alteration of bone metabolism<sup>63</sup>. In contrast, no relationship was found between ALP and bone density in elderly men, suggesting that ALP was not useful for monitoring bone integrity<sup>64</sup>, while no correlations were found between levels of osteocalcin and bone alkaline phosphatase in healthy and postmenopausal osteoporotic women<sup>65</sup>. The results of the present study showed that plasma ALP levels were elevated in PCOS-induced animals. In addition, the animals induced to PCOS presented greater bone fragility, as shown by the reductions of both maximum load and maximum load at the fracture point. Taken together with the plasma T and osteocalcin levels, the data suggested that in this EV-induced PCOS animal model, the hormone changes led to impaired bone metabolism.

Cells are substrate-smart and will use any fuel available during tissue culture<sup>66</sup>. The artificial environment in which in vitro studies are conducted can provide valuable insights. The osteogenic differentiation potential of cultured bone mesenchymal stem cells changes with the age of the donor and the treatment applied both in vivo and in vitro by means of cellular subculture. The expression of growth factors and increased bone matrix production was found to favor osteogenesis, improving the structural and mechanical properties of bone in exercised aged animals<sup>67-68</sup>. The mesenchymal stem cells used in the present study were obtained from the femurs bone marrow of adult rats. The cells remained viable throughout the in vitro experimental period and differentiated into osteoblasts. However, the cells obtained from the rats induced to PCOS exhibited decreased potential for osteoblastic differentiation and reduced viability, compared to the control animals. In this way, the bone alterations observed using in vivo studies can be explained, at least in part, by using in vitro results. The evidence suggests that lower osteoblast viability and mineralization are likely to among the mechanisms contributing to higher risk of fractures in women with PCOS.

In conclusion, the use of animal models and culture cells studies, such as those described in the present work are required for evaluation of different aspects of the etiology and pathophysiology of PCOS.

### **Acknowledgments**

We thank Aline C. Bertato and Ruither O.G. Carolino for technical support.

### **Author contributions**

L.H.M. and A.L.O.B. conceived and designed the research. A.L.O.B., E.D.A., and V.F. developed the experiments. K.O.N. and J.A.A.F. performed the bone and hormonal assay experiments, respectively. J.A.A. performed the statistical analyses of the data. L.H.M., A.L.O.B., E.D.A., V.F., K.O.N., J.A.A.F., and J.A.A. discussed the results and contributed to the final manuscript.

### **Funding sources**

The author A.L.O.B. was supported in part by the Coordenação de Aperfeiçoamento de Pessoal de Nível Superior – Brasil (CAPES). The author L.H.M. was supported by the São Paulo Research Foundation (FAPESP), SP, Brazil [grant number: 2016/02811-4].

### **References**

[1]. Preppard HR, Marfori J, Iutorno MJ, Nestler JE. “Prevalence of polycystic ovary syndrome among premenopausal

- women with type 2 diabetes" *Diabetes Care*, vol. 24, n° 6, pp. 1050–1052, 2001.
- [2]. Chen X, Yang D, Mo Y, Li L, Chen Y, Huang Y. "Prevalence of polycystic ovary syndrome in unselected women from southern China" *Eur J Obstet Gynecol Reprod Biol*, vol. 139, n° 1, pp. 59–64, 2008.
- [3]. March WA, Moore VM, Willson KJ, Phillips DI, Normal RJ, Davies MJ. "The prevalence of polycystic ovary syndrome in a community sample assessed under contrasting diagnostic criteria" *Hum Reprod*, vol. 25, n° 2, pp. 544–551, 2010.
- [4]. Fause BC, Tarlatzis BC, Rebar RW, Legro RS, Balen AH, Lobo R, Carmina E, Chang J, Yildiz BO, Laven JS, Boivin J, Petraglia F, Wijeyratne CN, Norman RJ, Dunaif A, Franks S, Wild RA, Dumesic D, Barnhart K. "Consensus on women's health aspects of polycystic ovary syndrome (PCOS): the Amsterdam ESHRE/ASRM-Sponsored 3<sup>rd</sup> PCOS Consensus Workshop Group" *Fertil Steril*, vol. 97, n° 1, pp. 28–38, 2012.
- [5]. Noroozadeh M, Behboudi-Gandevani S, Zadeh-Vakili A, Tehrani FR. "Hormone-induced rat model of polycystic ovary syndrome: A systematic review" *Life Science*, vol. 191, pp. 259–272, 2017.
- [6]. Torres PJ, Siakowska M, Banaszewska B, Pawelczyk L, Duleba AJ, Kelley ST Thackray VG. "Gut microbial diversity in women with polycystic ovary syndrome correlates with hyperandrogenism" *J Clin Endocrinol Metab*, vol. 103, n° 4, pp. 1502–1511, 2018.
- [7]. Dunaif A. "Insulin resistance and the polycystic ovary syndrome: mechanism and implications for pathogenesis" *Endocr Revi*, vol. 18, n° 6, pp. 774–800, 1997.
- [8]. Franks S. "Does animal model of polycystic ovary syndrome help to understand its pathogenesis and management? Yes, but their limitations should be recognized" *Endocrinology*, vol. 150, n° 9, pp. 3983–3985, 2009.
- [9]. Moran LJ, Misso ML, Wild RA, Norman RJ. "Impaired glucose tolerance, type-2 diabetes and metabolic syndrome in polycystic ovary syndrome: a systematic review and meta-analysis" *Hum Reprod Update*, vol. 16, n° 4, pp. 347–363, 2010.
- [10]. Wu XY, Li ZL, Wu CY, Lin YM, Lin H, Wang SH, Xiao WF. "Endocrine traits of polycystic ovary syndrome in prenatally androgenized female Sprague-Dawley rats" *Endocr J*, vol. 57, n° 3, pp. 201–209, 2010.
- [11]. Goodarzi MO, Dumesic DA, Chazenbalk G, Azziz R. "Polycystic ovary syndrome: etiology, pathogenesis and diagnosis" *Nat Rev Endocrinol*, vol. 7, n° 4, pp. 219–231, 2011.
- [12]. Macut D, Bjekic-Macut J, Savic-Radojevic A. "Dyslipidemia and oxidative stress in PCOS" *Front Horm Res*, vol. 40, pp. 51–63, 2013.
- [13]. Ali A. "Polycystic ovary syndrome and metabolic syndrome" *Ceska Gynekol*, vol. 80, pp. 279–289, 2014.
- [14]. Azziz R, Carmina E, Chen ZJ, Dunaif A, Laven JSE, Legro RS, Lizneva, Natterson-Horowitz B, Teede HJ, Yildiz BO. "Polycystic ovary syndrome" *Nat Rev*, vol. 2, pp. 1–18, 2016.
- [15]. Alves ED, Bonfá ALO, Pigatto GR, Anselmo-Franci JA, Achcar JA, Parizotto NA, Montezor LH. "Photobiomodulation can improve ovarian activity in polycystic ovary syndrome-induced rats" *Journal of Photochemistry & Photobiology, B: Biology*, vol. 194, pp. 6–13, 2019.
- [16]. Carreau AM, Jin ES, Garcia-Reyes Y, Rahat H, Nadeau KJ, Malooy CR, Cree-Green M. "A simple method to monitor hepatic gluconeogenesis and triglyceride synthesis following oral sugar tolerance test in obese adolescent" *Am J Physiol Regul Integr Comp Physiol*, vol. 317, pp. R134–R142, 2019.
- [17]. Diamanti-Kandaraki E, Spina G, Kouli C, Migdalis. "Increased endothelin-1 levels in women with polycystic ovary syndrome and the beneficial effect of metformin therapy" *J Clin Endocrinol Metab*, vol. 86, pp. 4666–4673, 2001.
- [18]. Wenner MM, Taylor HS, Stachenfeld NS. "Androgens influence microvascular dilation in PCOS through ET-A and ET-B receptors" *Amer J Physiol Endocrinol Metab*, vol. 305, pp. E818–E825, 2013.
- [19]. Krishnan A, Muthusami S. "Hormonal alterations in PCOS and its influence on bone metabolism" *J Endocrinol*, vol.

232, pp. R99–R113, 2017.

- [20]. Usselman CW, Yarovinsky TO, Steele FE, Leone CA, Taylor HS, Bender JR, Stachenfeld NS. “Androgens drive microvascular endothelial dysfunction in women with polycystic ovary syndrome: role of the endothelin B receptor” *J Physiol*, vol. 597, n° 11, pp. 2853–2865, 2019.
- [21]. Astapova O, Minor BMN, Hammes SR. “Physiological and pathological androgen actions in the ovary” *Endocrinology*, vol. 160, n° 5, pp. 1166–1174, 2019.
- [22]. Abu EO, Horner A, Kusec V, Triffitt JT, Compston JE. “The localization of androgen receptor in bone” *J Clin Endocrinol Metab*, vol. 82, pp. 3493–3497, 1997.
- [23]. Zborowski JV, Evelyn O, Talbott, Jane AC. “Polycystic ovary syndrome, androgen excess and impact on the bone” *Obstetrics and Gynecology Clinics*, vol. 8, pp. 131–151, 2000.
- [24]. Tamadon A, Hu W, Cui P, Ma T, Tong X, Zhang F, Li X, Shao LR, Feng Y. “How to choose the suitable animal model of polycystic ovary syndrome?” *Trad Med Mod Med*, vol. 1, n° 2, pp. 95–113, 2018.
- [25]. Kosłowska A, Wojtkiewicz J, Majewski M, Jana B. “The noradrenergic innervation and steroidogenic activity of porcine cystic ovaries” *Physiol Res*, vol. 62, pp. 421–433, 2013.
- [26]. Pan JX, Zhang JY, Ke ZH, Wang FF, Barry JA, Hardiman PJ, Qu F. “Androgens as double-edged swords: Induction and suppression of follicular development” *Hormones*, vol. 14, n° 2, pp. 190–200, 2015.
- [27]. Chuffa LGDA, Lupi Júnior LA, da Maia Lima AF. “Sex steroid receptors and apoptosis-related protein are differentially expressed in polycystic ovaries of adult dogs” *Tissue Cell*, vol. 48, pp. 10–17, 2016.
- [28]. Jia L, Li, J, He B, Jia Y, Niu Y, Wang C, Zhao R. “Abnormally activated one-carbon metabolic pathway is associated with mtDNA hypermethylation and mitochondrial malfunction in the oocyte of polycystic gilt ovaries” *Sci Rep*, vol. 6, pp. 19436, 2016.
- [29]. Ryu Y, Kim SW, Kim YY, Ku SY. “Animal model for human polycystic ovary syndrome (PCOS) focused on the use of indirect hormonal perturbations: A review of the literature” *Int J Molec Sci*, vol. 20, pp. 1–27, 2019.
- [30]. Brawer JR. “Development of the polycystic ovarian condition (PCO) in the estradiol valerate-treated rat” *Biol Reprod*, vol. 35, n° 3, pp. 647–655, 1986.
- [31]. Montrezor LH, Carvalho D, Dias MB, Anselmo-Franci JA, Bicego KC, Gargaglioni LH. “Hypoxic and hypercapnic ventilatory responses in rats with polycystic ovaries” *Resp Physiol Neurobiol*, vol. 217, pp. 17–24, 2015.
- [32]. Pereira VM, Honorato-Sampaio K, Martins AS, Reis FM, Reis AM. “Downregulation of natriuretic peptide system and increased steroidogenesis in rat polycystic ovary” *Peptides*, vol. 60, pp. 80–85, 2014.
- [33]. Muhammad SI, Maznah I, Mahmud RB, Esmail MF, Zuki ABZ. “Bone mass density estimation: Archimede’s principle versus automatic X-ray histogram and edge detection technique in ovariectomized rats treated with germinated brown rice bioactives” *Clinical Intervention in Aging*, vol. 8, pp. 1421–1431, 2013.
- [34]. Martin RB. “Effects of stimulated weightlessness on bone properties in rats” *Journal of Biomechanics*, vol. 23, n° 10, pp. 1021–1029, 1990.
- [35]. Wang H, Chen Q, Lee SH, Choi Y, Johnson FB, Pignolo RJ. “Impairment of osteoblast differentiation due to proliferation-independent telomere dysfunction in mouse models of accelerated aging” *Aging Cell*, vol. 11, n° 4, pp. 704–713, 2012a.
- [36]. Maniopoulos C, Sodek J, Melcher AH. “Bone formation in vitro by stromal cells obtained from bone marrow of young adult rats” *Cell and Tissue Research*, vol. 254, n° 2, pp. 317–330, 1988.
- [37]. Mosmann T. “Rapid colorimetric assay for cellular growth and survival: Application to proliferation and cytotoxicity assays” *J Immunol Meth*, vol. 65, n° 1–2, pp. 55–63, 1983.

- [38]. Gregory CA, Gunn WG, Peister A, Prockop DJ. "An Alizarin red-based assay of mineralization by adherent cells in culture: comparison with cetylpyridinium chloride extraction" *Analytical Biochemistry*, vol. 329, n° 1, pp. 77–84, 2004.
- [39]. Walters KA, Allan CM, Handelsman DJ. "Rodent models for human polycystic ovary syndrome" *Biol Reprod*, vol. 86, n° 5, pp. 1–12, 2012.
- [40]. Lyon MF, Glenister PH. "Reduce reproductive performance in androgen-resistant Tfm/Tfm female mice" *Proc R Soc Lond B Biol Sci*, vol. 208, pp. 1–12, 1980.
- [41]. Kozłowska A, Majewski M, Jana B. "Expression of steroidogenic enzymes in porcine polycystic ovaries" *Fol Histochem Cytobiol*, vol. 47, n° 2, pp. 257–264, 2009.
- [42]. Baptiste CG, Battista MC, Trottier A, Ballargeon JP. "Insulin and hyperandrogenism in women with PCOD" *J Ster Biochem Mol Biol*, vol. 122, pp. 1–22, 2010.
- [43]. Chen MJ, Chou CH, Chen CU, Yang WS, Yang YS, Ho HN. "The effect of androgens on ovarian follicle maturation: Dihydrotestosterone suppress FSH-stimulated granulosa cell proliferation by upregulating PPAR $\mu$ -dependent PTEN expression" *Scientific Reports*, vol. 5, n° 18319, 2015.
- [44]. Abbott DH, Barnett DK, BReiuns CM, Dumestic DA. "Androgens excess fetal programming of female reproduction: a developmental aetiology for polycystic ovary syndrome?" *Hum Reprod Update*, vol. 11, n° 4, pp. 357–374, 2005.
- [45]. Hsueh AJ, Billig H, Tsafiri A. "Ovarian follicle atresia: a hormonally controlled apoptotic process" *Endocr Rev*, vol. 15, pp. 707–724, 1994.
- [46]. Kaipia A, Hsueh AJ. "Regulation of ovarian follicle atresia" *Ann Rev Physiol*, vol. 59, pp. 349–363, 1997.
- [47]. Lin TT, Chang HM, Hu XL, Leung PCK, Zhu YM. "Follicular localization of growth differentiation factor 8 and its receptors in normal and polycystic ovary syndrome" *Biol Reprod*, vol. 98, n° 5, pp. 683–694, 2018.
- [48]. Zeleznik AJ, Hillier SG, Ross GT. "Follicle stimulating hormone-induced follicular development: an examination of the role of androgens" *Biol Reprod*, vol. 21, pp. 673–681, 1979.
- [49]. Bagnell CA, Mills TM, Costoff A, Mahesh VB. "A model for the study of androgen effects on follicular atresia and ovulation" *Biol Reprod*, vol. 27, pp. 903–914, 1982.
- [50]. McGee EA, Hsueh AJ. "Initial and cyclic recruitment of ovarian follicles" *Endocr Rev*, vol. 21, pp. 200–214, 2000.
- [51]. Andersen CY. "Characteristic of human follicular fluid associated with successful conception after in vitro fertilization" *J Clin Endocrinol Metab*, vol. 77, p.1227–1234, 1993.
- [52]. Nelson VL, Legro RS, Strauss JF, Mcallister JM. "Augmented androgen production is a stable steroidogenic phenotype of propagated theca cells from polycystic ovaries" *Mol Endocrinol*, vol. 13, pp. 946–957, 1999.
- [53]. Bilezikian JP, Morishima A, Bell J. "Increased bone mass as a result of estrogen therapy in a man with aromatase deficiency" *NEJM*, vol. 339, pp. 599–603, 1998.
- [54]. Lin IC, Slemper AE, Hwang C, Sena-Esteves M, Nah HD, Kirschner RE. "Dihydrotestosterone stimulates proliferation and differentiation of fetal calvarial osteoblast and dural cells and induces cranial suture fusion" *Plastic and Reconstructive Surgery*, vol. 120, pp. 1137–1147, 2007.
- [55]. Sawalha AH, Kovats S. "Dehydroepiandrosterone in systemic lupus erythematosus" *Current Rheumatology Reports*, vol. 4, pp. 286–291, 2008.
- [56]. Ferron M, Lacombe J. "Regulation of energy balance by skeleton: osteocalcin and beyond" *Arch Biochem Biophys*, vol. 561, pp. 137–146, 2014.
- [57]. Verbicaro, T, Giovanini, AF, Zielak, JC, Filho, FB, Araújo, MR, Deliberador, TM. "Osteocalcin immunohistochemical expression during repair of critical-sized bone defects treated with subcutaneous adipose tissue in rat and rabbit

animal model” Brazilian Dental Journal, vol. 24, n° 6, pp. 559–564, 2013.

- [58]. Moser SC, van der Eerden BCJ. “Osteocalcin – A versatile bone–derived hormone” *Frontier Endocrinol*, vol. 9, pp. 794–800, 2019.
- [59]. Zhong N, Xu B, Cui R, Xu M, Su J, Zhang Z, Liu Y, Li L, Sheng C, Qu SS. “Positive correlation between serum osteocalcin and testosterone in male hyperthyroidism patients with high bone turnover” *Exp Clin Endocrinol Diabetes*, vol. 124, n° 7, pp. 452–456, 2016.
- [60]. Bolland MJ, Grey A, Horne AM, Reid IR. “Testosterone levels following decreased in serum osteocalcin” *Calc Tissue Intern*, vol. 93, pp. 133–136, 2013.
- [61]. Oury F, Ferron M, Huizhen W. “Osteocalcin regulates murine and human fertility through a pancreas–bone–testis–axis” *J Clin Invest*, vol. 123, pp. 2421–2433, 2013.
- [62]. Lin SM, Kim YN, Park KH, Kang B, Chon HJ, Kim C, Kim JH, Rha SY. “Bone alkaline phosphatase as a surrogate marker of bone metastasis in gastric cancer patients” *MC Cancer*, vol. 16, pp. 385, 2016.
- [63]. Chen H, Li J, Wang Q. “Associations between bone–alkaline phosphatase and bone mineral density in adults with and without diabetes” *Medicine*, vol. 97, n° 17, n° e0432, 2018.
- [64]. Lumachi F, Orlando R, Fallo F, Basso SMM. “Relationship between bone formation markers bone alkaline phosphatase, osteocalcin and amino–terminal propeptide of type–I collagen and bone mineral density in elderly men. Preliminary results” *In vivo*, vol. 26, pp. 1041–1044, 2012.
- [65]. Diego EMD, Martin MAD, de la Piedra C, Rapado A. “Lack of correlation between levels of osteocalcin and bone alkaline phosphatase in healthy control and postmenopausal osteoporotic women” *Horm Metab Res*, vol. 27, pp. 151–154, 1994.
- [66]. Lee WC, Guntur AR, Long F, Rosen CJ. “Energy metabolism of the osteoblast: Implications for osteoporosis” *Endocrine Review*, vol. 38, pp. 255–266, 2017.
- [67]. Brancaglião LFC, Bonfá, ALO, Lemos JES, Rocha NF, Gonçalves VM, Montezor LH. “Effects of ovarian steroids on osteoblast viability and mineralization” *Asian J Biol*, vol. 2, n° 3, pp. 1–18, 2017.
- [68]. Singulani, MP, Stringhetta–Garcia CT, Santos LF, Morais SRL, Louzada MJQ, Oliveira, SHP, Neto AHC, Dornelles, RCM. “Effects of strength training on osteogenic differentiation and bone strength in aging female Wistar rats” *Scientific Report*, vol. 7, n° 42878, 2017.



## Study of ph effect on AZ31 magnesium alloy corrosion for using in temporary implants

CAJ. da Silva<sup>1</sup>; LNM. Braguin<sup>1</sup>; LO. Berbel<sup>1</sup>; BVG. de Viveiros<sup>1</sup>; JL. Rossi<sup>1</sup>; M. Saiki<sup>1</sup>; I. Costa<sup>1</sup>

\*Corresponding author: E-mail address: [caio.silva@ipen.br](mailto:caio.silva@ipen.br)

**Abstract:** Currently, magnesium alloys are gaining great interest for medical applications due to their degrading properties in the human body ensuring a great biocompatibility. These alloys also provide profitable mechanical properties due similarities with human bone. However, a difficulty in applying these materials in the biomaterials industries is the corrosion prior to cell healing. The effect of the chemical composition of Mg alloys on their corrosion behavior is well known. In this study, samples of AZ31 magnesium alloy were cut into chips for elemental chemical analysis by neutron activation analysis (NAA). Concentrations of the elements As, La, Mg, Mn, Na, Sb and Zn were determined in the AZ31 alloy. Visualization tests of agar corrosion development in various media, of 0.90% sodium chloride solution (mass), phosphate buffer saline (PBS) and simulated body fluid (SBF) were performed. Visualizations of the effect of agar gel corrosion revealed pH variation during the corrosion process due to the released into the cathode. The highest released of hydroxyl ions occurred in NaCl solution compared to PBS and SBF solutions indicating that NaCl solution was much more aggressive to the alloy compared to the others.

**Keywords:** Biomaterials. Magnesium alloy. Neutron activation analysis. Corrosion.

### Introduction

Considering the increase of biomaterials industry, the scientific community has searched about development of new types of these materials for biomedical applications, as well as for the improvement of the existing ones. Among these biomaterials, magnesium alloys have been proposed in this scenario as biodegradable metals for temporary implants, which avoids a new surgery for their removal<sup>1</sup>, in the applications as cardiovascular stents and orthopedic prostheses.

This applicability is mainly due its intrinsic biocompatibility in the physiological environment since the major element (Mg) is a cofactor of more than 300 enzymatic reactions in the body, such as DNA, RNA and protein synthesis<sup>2</sup>. Several studies have also reported additional benefits of magnesium such as antibacterial, osteoconductor and osteoinductor effect<sup>3</sup>.

Moreover, these alloys provide mechanical properties similar to the human bone which also avoids stress shielding phenomena<sup>4</sup>. However, magnesium alloys can quickly dissolve and corrode in aqueous solutions; especially those containing chloride ions<sup>5</sup>.

Rapid degradation rates in physiological medias are the main limitation for the use of these magnesium alloys, essentially in cases of degradation before cell healing<sup>6-8</sup>. Concerning to alloy elements and its impurities, it is known that they can form secondary particles, which may be nobler than the matrix, facilitating or inhibiting the degradation rate<sup>9</sup>.

The main chemical reactions that occur by Mg in contact with physiological media in the body are anodic reaction of Mg oxidation (1) and cathodic reaction of water reduction (2)<sup>2</sup>:



According to the reaction (2), Mg corrosion causes variation of the pH on the medium. Corrosion monitoring by means of pH measurements has been widely used in the study of magnesium degradation, although this kind of analysis usually brings only qualitative results. This is the cathodic reaction (Eq. 2) that can be used as an estimate to predict the overall corrosion rate based on the measurement of pH increase<sup>9</sup>.

Neutron Activation Analysis (NAA) was the analytical technique used to determine elements in this study to analyze Mg alloy composition, due to its advantages in the analysis of this type of materials such as high sensitivity, multi-element determination and the analyses of a great variety of matrices<sup>10</sup>.

The objective of this research was to determine the elemental composition of the AZ31 magnesium alloy by the NAA technique as well as to evaluate the variation of pH during the corrosion of this alloy in different simulated body solutions.

## MATERIALS AND METHODS

### Materials

The AZ31 magnesium alloy studied was imported to Alfa Aesar from Massachusetts, United States. This alloy was acquired in foil form with dimensions 30 cm x 30 cm and 1 mm thickness.

The preparation of the alloy for element determination

<sup>1</sup>Instituto de Pesquisas Energéticas e Nucleares (IPEN – CNEN/SP)

was firstly to transform it in the form of chips with the aid of steel pliers. The cleaning of the chips to eliminate possible contaminants from the steel pliers was performed using acetone PA in beaker containing the chips and under agitation with a glass stick. The chips were separated from acetone. Then the purified water was added to the beaker, where alloy chips remained immersed for about two hours. The separation of the chips of the solution was carried out by filtration with filter paper. The filter paper containing the chips was put in a Petri dish, which was placed inside the laminar flow cabin for drying at room temperature.

Figure 1 shows the photograph of AZ31 alloy chips of dimensions of 0.2 to 1.0 cm used in the analysis.

The alloy sample for corrosion immersion tests was obtained by cutting the alloy with dimensions of 15 mm x 15 mm using a mechanical guillotine. Then the samples were submitted to cleaning using successively ethyl alcohol, acetone and purified water under agitation for about 15 minutes, in each of the reagents. To obtain smooth and uniform surfaces, the alloys were grinded using silicon carbide paper of #500, #800, #1200, #2000 and #4000 granulometry successively. Ethyl alcohol was used to clean the alloy surface between the steps of the grinding and, in the final steps, with distilled water followed by drying with hot air jet.



**Figure 1.** Photograph of the chips obtained from AZ31 alloy.

**Source:** CAJ, Silva.

Simulated body solutions were used in *in vitro* tests of the electrochemical reactions with the AZ31 magnesium alloy. The solutions of 0.90% sodium chloride (mass), phosphate buffered saline (PBS) and simulated body fluid (SBF) are those commonly used in this corrosion studies of biomaterials<sup>11-13</sup> and were adopted in this work. The reagents used in the preparation of these solutions are presented in Table 1.

The PBS solution was prepared using 9.0 g of sodium chloride, 1.42 g of dibasic sodium phosphate and 2.72 g of monobasic potassium phosphate dissolved and diluted to 1000 mL of purified water. Regarding to SBF solution, its preparation was carried out according to Kokubo e Takadama<sup>14</sup> with the exception of the water used, the purified water in the Millipore purification system was used instead of distilled water.

## Methods

### Procedure of neutron activation analysis (NAA)

For NAA, 50 mg of alloy chips were weighed in polyethylene envelopes and irradiated in the IEA-R1 reactor along with synthetic element standards. These standards were prepared pipetting single or multielemental standard solutions in sheets of filter paper.

Details about experimental procedure used for NAA as well as about analytical quality control of the results are presented in a previous work<sup>15</sup>.

The concentrations of the elements were calculated by the comparative method<sup>16</sup> using the following equations.

$$C_a = \frac{m_p \cdot A_a \cdot e^{0,693(ta-tp)t_{1/2}}}{M_a \cdot A_p} \quad (3)$$

where  $C_s$  is the element concentration in the sample;  $m_{st}$  is the mass of the element in the standard;  $A_s$  and  $A_{st}$  are counting rates of the radioisotopes in the sample and in the standard, respectively;  $t_s$  and  $t_{st}$  are decay times for the sample and standard, respectively;  $M_s$  is the total mass of the sample and  $t_{1/2}$  is the half-life of the radionuclide.

**Table 1.** Reagents used in the preparation of the simulated body solutions of 0.90% in mass of NaCl, phosphate buffered saline (PBS) and simulated body fluid (SBF).

Solution	Reagents	Molecular formula	Purity (%)
NaCl/ PBS/ SBF	Sodium chloride	NaCl	≥99.0
SBF	Potassium chloride	KCl	≥99.0
PBS	Bibasic sodium phosphate	Na <sub>2</sub> HPO <sub>4</sub>	≥99.0
PBS	Monobasic sodium phosphate	KH <sub>2</sub> PO <sub>4</sub>	≥99.0
SBF	Sodium hydrogen carbonate	NaHCO <sub>3</sub>	≥99.7
SBF	Tri-hydrated potassium phosphate	K <sub>3</sub> PO <sub>4</sub> · 3 H <sub>2</sub> O	≥99.0
SBF	Hexahydrate magnesium chloride	MgCl · 6 H <sub>2</sub> O	≥99.0
SBF	Hydrochloric acid	HCl	36.5 – 38
SBF	Calcium chloride	CaCl <sub>2</sub>	≥96.0
SBF	Sodium sulfate	Na <sub>2</sub> SO <sub>4</sub>	≥99.0
SBF	Tris-hydroxymethyl aminomethane (Tris)	C <sub>4</sub> H <sub>11</sub> NO <sub>3</sub>	≥99.0

**Procedure used for corrosion visualization test in agar-agar gel**

Firstly, the areas of the alloy samples to be exposed to corrosion were delimited to 1 cm<sup>2</sup> using biological wax to avoid preferential corrosion at the edges (crevice). The agar-agar used was the bacteriological type of Kasvi K25-1800 and for its preparation 1.5 grams of agar-agar was used for 50 mL solution<sup>17</sup>.

For this preparation, each one of the solutions (0.90% in mass of NaCl, PBS and SBF) was heated to boiling temperature (100 ± 2) °C in a beaker of 50 mL. In this heated solution, 1.5 g of agar-agar and 5 mL of phenolphthalein indicator were added and with the aid of a glass stick, the solutions were homogenized and transferred into a Petri dish containing an alloy sample.

**Procedure for corrosion monitoring by global pH measurement**

The pH variation of the solution in contact with magnesium alloy sample was performed for different times at room temperature. For this, alloy samples with an area of 2.2 cm<sup>2</sup> were immersed in each one of the solutions NaCl, PBS and SBF. The test was performed in plastic Falcom tube with the capacity of 15 mL and the volume of each solution was of 11 mL. The ratio between solution volume and exposed alloy area was 5 mL/cm<sup>2</sup>.

The pH measurements were performed using KASVI K39-2014B bench-type pHmeter and this test was performed in duplicate, and the mean value of pH measurements was used in the evaluation.

**RESULTS AND DISCUSSION****Element determination in the AZ31 magnesium alloy**

Table 2 shows the results of determinations in the AZ31 magnesium alloy sample by NAA, as well as the results of detection limit of Cu, Fe and Ni elements, not detected in the analysis. The detection limits of these three elements were evaluated since they are commonly present in metal alloys and, in addition the alloy specification sheet shows only their maximum values.

**Table 2.** Concentrations of elements obtained in the AZ31 magnesium alloy by NAA.

Element	M $\pm$ SD <sup>a</sup>	RSD <sup>b</sup> , %	Reference <sup>18</sup>
Al, %	3.06 $\pm$ 0.19	6.1	2.5 – 3.5
As, $\mu\text{g g}^{-1}$	2.30 $\pm$ 0.34	14.8	–
Cu, %	< 0.012	–	<0.05
Fe, %	< 0.095	–	<0.005
Mg, %	96.5 $\pm$ 4.2	4.4	Remainder
Mn, %	0.325 $\pm$ 0.013	3.9	0.2 – 1.0
Ni, %	< 0.037	–	<0.005
Na, $\mu\text{g g}^{-1}$	397 $\pm$ 32	8.1	–
Sb, $\text{ng g}^{-1}$	275 $\pm$ 56	20.4	–
La, $\text{ng g}^{-1}$	316 $\pm$ 16	5.2	–
Zn, %	1.009 $\pm$ 0.045	4.5	0.6 – 1.3

a. arithmetic mean and standard deviation from 2 to 4 determinations; b. relative standard deviation.

Table 2 shows that the concentrations of elements Al, Mn and Zn are within the ranges of specification/reference values and, in addition, four other elements were detected and quantified: As, Na, Sb and La. The relative standard deviations of the determinations were less than 15.0 %, with the exception of Sb, that presented RSD of 20.4 % due to its low concentration in the alloy.

### Results of the corrosion visualization tests in agar-agar gel

In Figures from 2 to 4, the images of corrosion visualization in agar-agar before and after exposure are presented with the test solutions containing phenolphthalein as the acid-base indicator.

For the test in sodium chloride solution, (Fig.2) the alloy is shown (a) prior to exposure to the test solution and, (b) after immersion. The pink coloration is due to the formation of hydroxyl ions (OH<sup>-</sup>) resulting from the cathodic reaction. The pink color is instantly evidenced in a large surface area, as well as the formation of H<sub>2</sub> bubbles. It can be seen that the pink coloration intensifies (after one hour) (c) and coloration propagates throughout the surface area (after two hours), (d).

In the PBS medium (Fig.3), in (a) the AZ31 alloy sample prior to immersion is shown, and large formation of H<sub>2</sub> bubbles is observed over much of the sample in (b), evidencing a high reactivity of the alloy in this medium. After five hours of test the H<sub>2</sub> bubbles remained(c). However, only after 24 hours of assay (d) a slight pink coloration was indicated due to low rates of cathodic oxygen reduction reaction.

As in previous cases, in the SBF medium (Fig.4) there is an instantaneous formation of H<sub>2</sub> bubbles on the surface and also the presence of pink staining regions in (b). The intensification of OH<sup>-</sup> formation gradually increased after one hour (c) and five hours of test (d), where the staining remained during 24-hour monitoring.

This visualization test allowed identifying the preferred cathodic regions in the early stages of corrosion from the main water reduction reaction (Eq. 2). It is noted in Fig 2 that in sodium chloride solution, after two hours of immersion, the identification and differentiation of the anodic and cathodic regions are hard to be identified due to intense corrosion attack and large release of hydroxyl ions.

### Results of corrosion monitoring by global pH measurements

The results of pH measurements in sodium chloride solution, PBS and SBF during 5 days of test in duplicate are shown in Figure 5. It is observed that the pH of the medium varies faster and more intensely in the case of the NaCl medium, showing that it corresponds to the most aggressive medium among the tested.

The curves of pH variation with exposure time in PBS and SBF solutions showed similar behavior for these solutions, i.e., continuous pH increase from the beginning to the end of test, generally in the order of 2 units. In the sodium chloride solution, the pH increase was about six pH units (from 4.43 to 10.79). Additionally, between 1 and 3 hours of test there was an abrupt and significant increase in pH. It should be noted that in SBF, the pH reached values close to those observed in the sodium chloride solution at the end of the test, after 5 days.

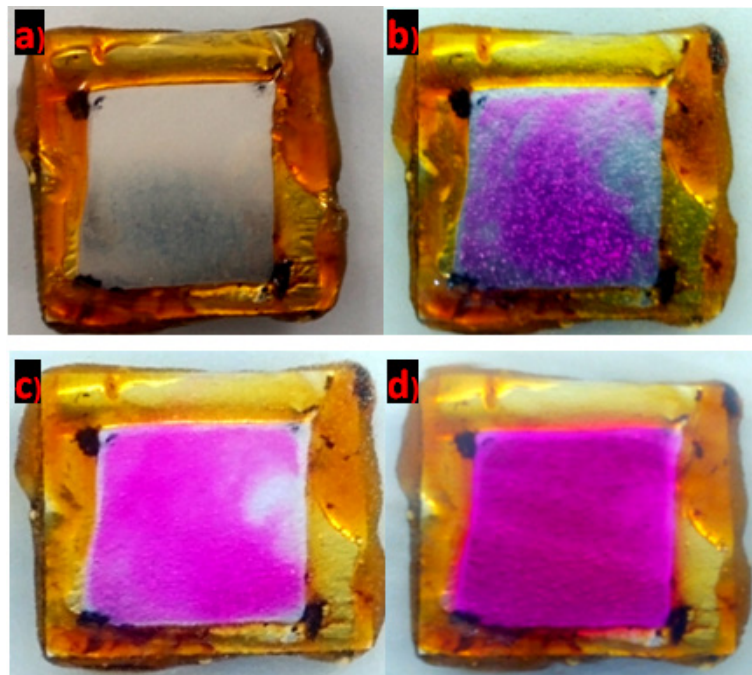


**Figure 2.** Photographs of the AZ31 alloy in 0.90 wt. % sodium chloride agar–agarcontaining phenolphthalein for different immersion periods; photos of sample (a) prior to immersion, (b) just after immersion, (c) after an hour of immersion and (d) after two hours of immersion.

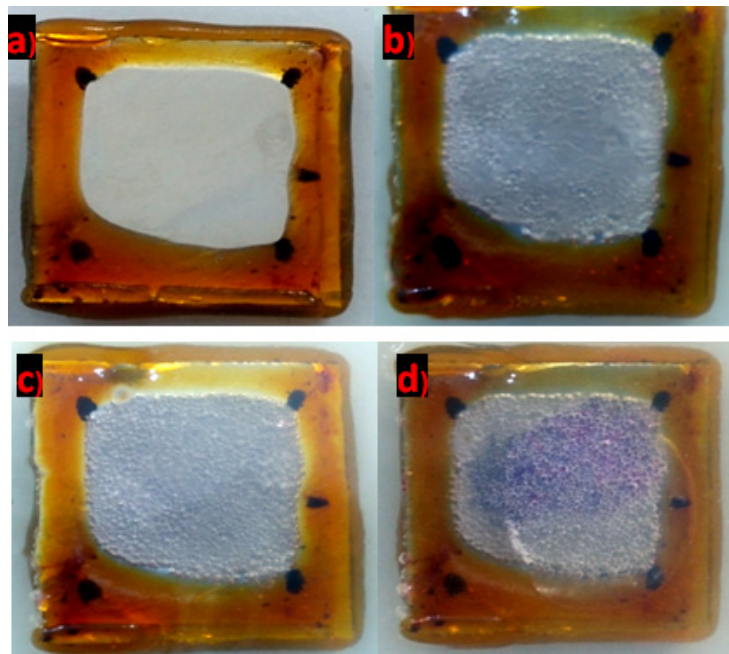


**Figure 3.** Photographs of the AZ31 alloy in PBS agar–agar containing phenolphthalein for different immersion periods; photos of sample (a) prior to immersion, (b) just after immersion, (c) after an hour of immersion and (d) after one day of immersion.

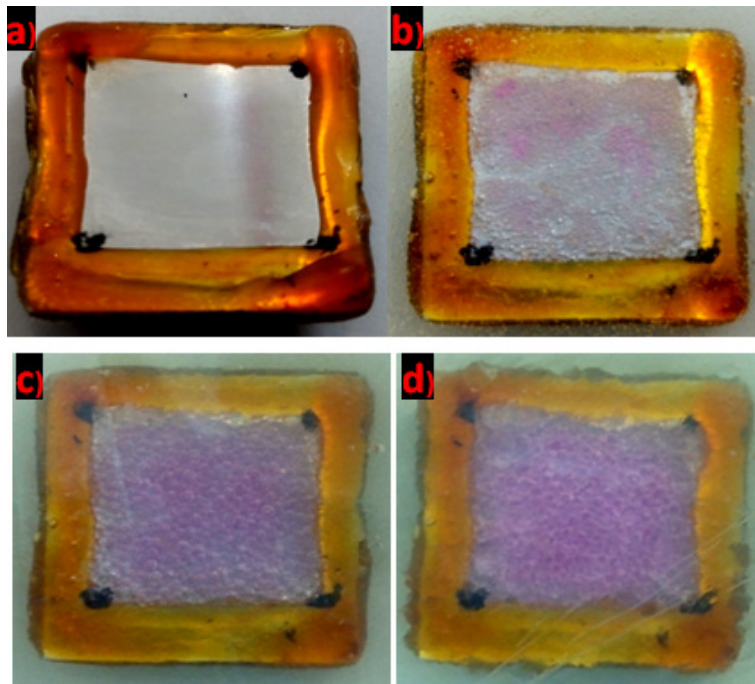


**Figure 4.** Photographs of the AZ31 alloy in SBF agar-agar containing phenolphthalein for different immersion times; photos of sample (a) prior to immersion, (b) just after immersion, (c) after an hour of immersion and (d) after five hours of immersion.

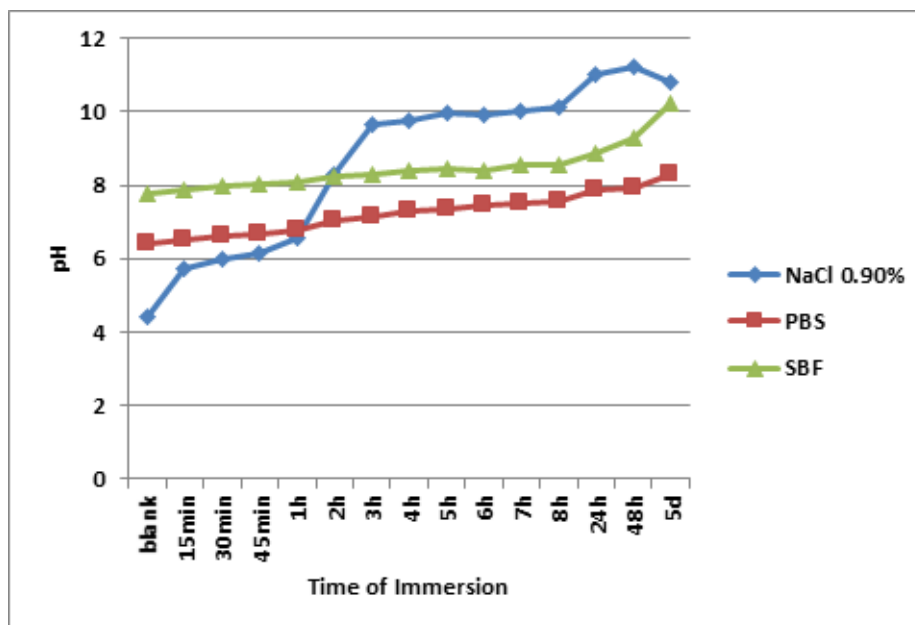


**Figure 5.** Curves of pH variation with time of exposure of AZ31 samples to simulated body solutions.

### Conclusions

Neutron activation analysis of AZ31 magnesium alloy showed that concentrations of Al, Mn and Zn are within the ranges stipulated by the supplier specification. Four elements (As, La, Sb and Na) not presented in this specification were determined by the NAA technique.

Visualization of color change in the agar-agar and the pH variation with time of test revealed high susceptibility of the tested alloy to corrosion since the first times of exposure and demonstrated a difference in intensity depending on the type of simulated body solution used. Sodium chloride solution was the medium with the highest activity resulting in the largest production of hydroxyl ions ( $\text{OH}^-$ ) among those produced in PBS and SBF solutions. On the other hand, the PBS solution was the least aggressive among the solutions tested.

### Acknowledgments

The authors are grateful to São Paulo Research Foundation (FAPESP–BRAZIL) and National Council for Scientific and Technological Development (CNPq–BRAZIL) for the financial support and the author C.A.J. Silva are also grateful to Co-ordination for the Improvement of Higher Education Personnel (CAPES–BRAZIL) for his grant.

## References

- [1]. Sezer N, Evis Z, Kayhan SMA, Koc Tahmasebifar M. Review of magnesium–based biomaterials and their applications. *J Magnes Alloy* 6: 23–43 (2018).
- [2]. Gu XN, Lo SS, Li XM., Fan YB. Magnesium based degradable biomaterials: a review. *Front Mater Sci* 8: 200–218 (2014).
- [3]. Jung O, Smeets R, Porchetta D, Kopp A, Ptock C, Müller U, Heiland M, Schwade M, Behr B, Kroeger N, Kluwe L, Hanken H, Hartjen P. Optimized in vitro procedure for assessing the cytocompatibility of magnesium–based biomaterials. *Acta Biomater* 23: 354–363 (2015).
- [4]. Shaw BA. Corrosion resistance of magnesium alloy in *ASM Handbook 13A – Corrosion: fundamentals, testing and protection*, ed by SD Cramer and BS Covino. ASM International, United States, p. 692 (2003).
- [5]. Ding W. Opportunities and challenges for the biodegradable magnesium alloys as next generation biomaterials. *Regen. Biomater*, 3: 79–86 (2016).
- [6]. Li X, Liu X, Wu S, Yeung KWK, Zheng Y, Chu PK. Design of magnesium alloys with controllable degradation for biomedical implants: from bulk to surface. *Acta Biomater* 45: 2–30 (2016).
- [7]. Tan L, Wang Q, Lin X, Wan P, Zhang G, Zhang Q, Yang K. Loss of mechanical properties in vivo and bone–implant interface strength of AZ31B magnesium alloy screws with Si–containing coating, *Acta Biomater* 10: 2333–2340 (2014).
- [8]. Pardo A, Merino MC, Coy AE, Arrabal R, Viejo F, Matykina E. Corrosion behavior of magnesium/aluminum alloys in 3.5% wt. NaCl. *Corros Sci* 50: 823–834 (2007).
- [9]. Kirkland N, Birbilis N, Staiger M. Assessing the corrosion of biodegradable magnesium implants: a critical review of current methodologies and their limitations. *Acta Biomater* 8: 925–936 (2012).
- [10]. Ehmman WD and Vance DE. *Radiochemistry and Nuclear Methods of Analysis*. 1st ed. John Wiley & Sons, Inc; New York, 1991. 560 p.
- [11]. Thirumalaikumarasamy D, Shanmugam K, Balasubramanian V. Comparison of the corrosion behaviour of AZ31B magnesium alloy under immersion test and potentiodynamic polarization test in NaCl solution, *J Magnes Alloy* 2: 36–49 (2014).
- [12]. Fue S, Gao H, Chen G, Gao L, Chen X. Deterioration of mechanical properties for pre–corroded AZ31 sheet in simulated physiological environment. *Mater Sci Eng*, 593: 153–162 (2014).
- [13]. Xue D, Yun Y, Tan Z, Dong, Z, Schulz MJ. In vivo and in vitro degradation behaviour of magnesium alloys as biomaterials, *J Mater Sci Technol* 28: 261–267 (2011).
- [14]. Kokubo T, Takadama H. How useful is SBF in predicting in vivo bone bioactivity? *Acta Biomater* 27: 2907–2915 (2006).
- [15]. Silva CAJ, Costa I, Rossi JL, Saiki M. Determination of chemical elements in magnesium–based materials by neutron activation analysis, *Proc. International Nuclear Atlantic Conference INAC 2019 Santos, Brazil* (2019).
- [16]. De Soete D, Gijbels R, Hoste J. *Neutron Activation Analysis*. Wiley–Interscience, London (1987).

- [17]. Bugarin AFS (2017). Study of corrosion resistance of 2024-T3 and 7475-T651 aluminium alloys by friction stir welding (FSW) [thesis]. São Paulo: Nuclear and Energy Research Institute; 2017.
- 18]. Alfa Aesar by Thermo Fisher Scientific. 44009 Magnesium Aluminum Zinc foil (2018), available at: <https://www.alfa.com/pt/catalog/044009/&gt> [accessed 5 July 2018].



# A study on corrosion resistance of ISO 5832-1 austenitic stainless steel used as orthopedic implant

LMN. Braguin<sup>1\*</sup>; CAJ. da Silva<sup>1</sup>; LO. Berbel<sup>1</sup>; BVG. de Viveiros<sup>1</sup>; JL. Rossi I<sup>1</sup>; Costa<sup>2</sup>; M. Saiki<sup>1</sup>

\*Corresponding author: e-mail address: [lilian.braguin@ipen.br](mailto:lilian.braguin@ipen.br)

**Abstract:** The ISO 5832-1 austenitic stainless steel used as biomaterial is largely applied in the area of orthopedics, especially in the manufacture of implants, such as temporary or permanent replacement of bone structures. The objective of this study was to evaluate the localized corrosion resistance of the ISO 5832-1 stainless steel used in orthopedic implants by electrochemical tests in two different solutions. The results of this study are of great interest to evaluate the corrosion of metallic implants that can result in the release of corrosion products into bodily fluids causing possible adverse biological reactions. The determination of the chemical elements in the composition of the ISO 5832-1 stainless steel was performed by neutron activation analysis (NAA). The samples for electrochemical tests were grinded with silicon carbide paper up to #4000 finishing, followed by mechanical polishing with diamond paste. The open circuit potential measurements and anodic polarization curves were obtained in solution of 0.90 wt. % of NaCl and of simulated body fluid (SBF). The results indicated that the ISO 5832-1 stainless steel presented a high resistance to crevice corrosion in simulated body fluid solution but high susceptibility to this form of corrosion in the chloride solution.

**Keywords:** Metallic biomaterials. Austenitic stainless steel. Localized corrosion. ISO 5832-1 alloy.

## Introduction

Biomaterials are described as “any substance (other than a drug) or combination of substances, synthetic or natural in origin, which can be used for any period of time, as a whole or as a part of a system which treats, augments, or replaces any tissue, organ, or function of the body”, by National Institutes of Health (NIH) from USA, according to Hastings<sup>1</sup>. Many definitions have been used for biomaterials, however the NIH definition is commonly the most accepted<sup>2</sup>.

Nowadays in the biomaterials industry, there is a growing variety of devices and materials that are being developed to be used in the treatment of diseases and injuries. Consequently, the definition of biomaterials has been expanded<sup>3</sup>.

Austenitic stainless steels (AISI 316L), mainly those produced according to ISO 5832-1<sup>4</sup>, have been used to meet the high demands for biomaterials for use in orthopedic prostheses due to their performance, mechanical strength and corrosion resistance when compared to titanium and Cr-Co alloys<sup>5</sup>. In medical field, austenitic stainless steels are widely used in plates (used in fracture treatment), screws, parts of total hip replacements, among others<sup>6</sup>.

In view of the above, there is a great interest to determine elements present in ISO 5832-1 stainless steel, as well as to evaluate the localized corrosion resistance when exposed in NaCl and simulated body fluid (SBF) solutions.

Several analytical techniques are applied in elemental analyses of metallic alloys, such as atomic absorption spectrometry (AAS)<sup>7</sup>, inductively coupled plasma atomic emission spectrometry (ICP-AES)<sup>8</sup>, UV-Visible spectrophotometry<sup>9</sup> and neutron activation analysis (NAA)<sup>9-12</sup>.

In this study, neutron activation analysis (NAA) was used due to its several advantages, such as high sensitivity for the detection of elements, multi-elemental determination, good precision and accuracy of the results

and this technique does not require the sample dissolution.

Among the studies about applications of NAA in the analyses of biomaterials, Cincu et al.<sup>13</sup> analyzed biomaterials used in dental clinics to verify the influence of corrosion products released of these materials on patient health. Their results of dental materials analyses indicated the presence of nickel that is an allergenic and toxic element, besides the results showed that these types of biomaterials were well tolerated by patients over a five-year period.

Giordano et al.<sup>14</sup> analyzed the electrochemical behavior of two biomaterials applied to orthopedic implants in 0.90 % sodium chloride (NaCl) solution. The materials analyzed were austenitic stainless steel according to ASTM F 138 and ISO 5832-9. The polarization tests presented that the ASTM F 138 steel is less corrosion resistant than the ISO 5832-9 steel. The higher corrosion resistance of ISO 5832-9 stainless steel is due to increase stability of the passive film and the high tendency to repassivate.

The objective of this study was to determine elemental concentrations in ISO 5832-1 stainless steel and to evaluate its localized corrosion resistance in 0.90 % of NaCl and body fluid simulated solutions by electrochemical tests.

## EXPERIMENTAL

### Neutron activation analysis (NAA) procedure

Samples of ISO 5832-1 austenitic stainless steel were purchased in the form of bar from Villares Metals S/A. For neutron activation analysis of the steel, sample was obtained in the form of chips (smaller than 1 cm).

These chips form was cleaned to eliminate eventual impurities originating from the equipment used for cutting the material.

To apply the comparative method of NAA, synthetic elemental standards were prepared. The certified standard solutions of the elements provided by Spex CertiPrep Chemical USA were diluted and single or multielement

<sup>1</sup>Institute for Energy and Nuclear Research (IPEN – CNEN/SP)

solutions were prepared. Aliquots of these solutions were pipetted onto sheets of Whatman filter paper.

NAA procedure used is described in a previous work of Braguin<sup>15</sup>. For irradiation, about 50 mg of the sample were weighed in polyethylene envelopes.

In the short irradiation procedure, sample and elemental standards were placed in a new polyethylene envelope positioned inside a polyethylene device and irradiated at the IEA-R1 reactor of the Institute for Energy and Nuclear Research for a period of 5 s under a thermal neutron flux of  $1.9 \times 10^{12} \text{ n cm}^{-2} \text{ s}^{-1}$ .

In the irradiations of 1 h, samples and synthetic standards were individually wrapped in aluminum foil, and irradiated in an aluminum device at the IEA-R1 reactor under a thermal neutron flux of  $4.5 \times 10^{12} \text{ n cm}^{-2} \text{ s}^{-1}$ .

Gamma ray activity measurements of radioisotopes were carried out using a GC3020 Model hyperpure germanium semiconductor detector coupled to a digital spectrum analyzer (DSA 1000), both from Canberra and a microcomputer. For data acquisition and its processing, the software Genie 2000 version 3.1 from Canberra was used. This program provides data of counting rates and gamma energies. The radioisotopes of the gamma spectra were identified by gamma ray energies and half-life. The elemental concentrations were calculated using the Equation (1)<sup>16</sup>.

$$C_s = [m_{st} \cdot A_s \cdot e^{0.693(tds - tdst)/t_{1/2}}] / [M_s A_{st}] \quad (1)$$

where the indices s and st refer to sample and standard, respectively;  $M_s$  = total sample mass;  $m_{st}$  = mass of the element in the standard;  $C_s$  = concentration of the element in the sample;  $t_{1/2}$  = half-life of the radioisotope considered;  $td$  = decay time;  $A_s$  = counting rates of the considered radioisotope in the sample for decay time  $tds$ ;  $A_{st}$  = counting rates of the considered radioisotope in the elemental standards for decay time  $tdst$ .

The quality control of the results was evaluated by the analysis of two certified reference materials, SRM 363 Steel Cr-V Modified, from the National Institute of Standards and Technology (NIST), USA<sup>17</sup> and the B.C.S/ S.S No. 467 Austenitic Stainless Steel from the BCS<sup>18</sup>. These results were presented in previous publication<sup>15</sup> and they showed good precision and accuracy, with relative standard deviations below 15.0% and values of  $|Zscore| \leq 2$  for most of elements.

### Treatment of the data obtained by neutron activation analysis

The results of the elemental concentrations in the alloy were evaluated calculating statistical parameters of arithmetic mean ( $\bar{x}$ ), standard deviation (SD) and relative standard deviation (RSD).

### Corrosion test procedure

For the corrosion study, the ISO 5832-1 austenitic stainless steel was cut to obtain the sample with the dimensions of 38 mm x 18 mm x 6 mm (length, width and thickness, respectively).

The sample for electrochemical tests was grinded with silicon carbide paper up to #4000 finishing, followed by mechanical polishing with 1  $\mu\text{m}$  diamond paste. After applying this polishing process, the sample was cleaned with alcohol, and then dried with a hot air jet.

The corrosion testing of ISO 5832-1 stainless steel was performed using the Gamry Reference 600+ equipment. The experimental arrangement of the electrochemical cell consisted of three electrodes, a platinum counter electrode, an Ag/AgCl (KCl 3M) reference electrode and a working electrode with exposure area of 0.5  $\text{cm}^2$ . A rod of polymeric material was placed to increase susceptibility to crevice corrosion.

The stainless steel sample was immersed in a volume of 40 mL of each type of electrolyte solution at room temperature. The electrolytes used were 0.90 % mass of NaCl solution and simulated body fluid (SBF) solution. The preparation of the SBF was performed according to the procedure described by Kokubo and Takadama<sup>19</sup>, but with the use of purified water instead of distilled water. The NaCl and SBF solutions were placed in polyethylene bottles and kept in a refrigerator.

The electrochemical tests used in this study were open circuit potential (OCP) measurements as a function of time of exposure to test solution and anodic polarization tests. The surface of stainless steel exposed to the corrosive medium was later analyzed by scanning electron microscopy (SEM).

## RESULTS AND DISCUSSION

Table 1 presents the results obtained from the analysis of ISO 5832-1 stainless steel using NAA. In this Table the mean elemental concentrations with their standard deviations, relative standard deviations, and sample specification data<sup>4</sup> are presented.

The concentrations of the elements Cr, Cu, Mn, Mo and Ni obtained in the ISO 5832-1 alloy are within of their specification range presented by ISO<sup>4</sup>. In this study As, Co, V and W elements not presented in the specification of this material were also determined. The results obtained for this alloy presented a relative standard deviation lower than 13.7 % indicating a good precision of the results.

**Table 1.** Concentrations of elements obtained for ISO 5832–1 austenitic stainless steel.

Element	( $\pm$ SD) <sup>a</sup>	RSD <sup>b</sup> , %	ISO 5832–1 <sup>4</sup>
As, $\mu\text{g g}^{-1}$	$15.0 \pm 1.5$	10.2	
Co, $\mu\text{g g}^{-1}$	$213.8 \pm 4.3$	2.0	
Cu, %	$0.0427 \pm 0.0025$	5.8	0.5 max
Cr, %	$17.06 \pm 0.61$	3.6	17.0 – 19.0
Fe, %	$62.6 \pm 2.1$	3.3	
Mn <sup>c</sup> , %	$1.60 \pm 0.12$	7.6	2.0 max
Mn <sup>d</sup> , %	$1.764 \pm 0.025$	1.4	2.0 max
Mo, %	$2.49 \pm 0.33$	13.3	2.25 – 3.00
Ni, %	$13.3 \pm 1.3$	9.5	13.0 – 15.0
V, $\mu\text{g g}^{-1}$	$352.5 \pm 7.9$	2.2	
W, $\mu\text{g g}^{-1}$	$110 \pm 15$	13.7	

a. arithmetic mean and standard deviation from 3 to 5 determinations, b. relative standard deviation, c. results of five-second irradiation, d. results of one-hour irradiation.

In the Figure 1 the open circuit potential variation curves for ISO 5832–1 austenitic stainless steel in 0.90% NaCl and SBF solutions are presented.

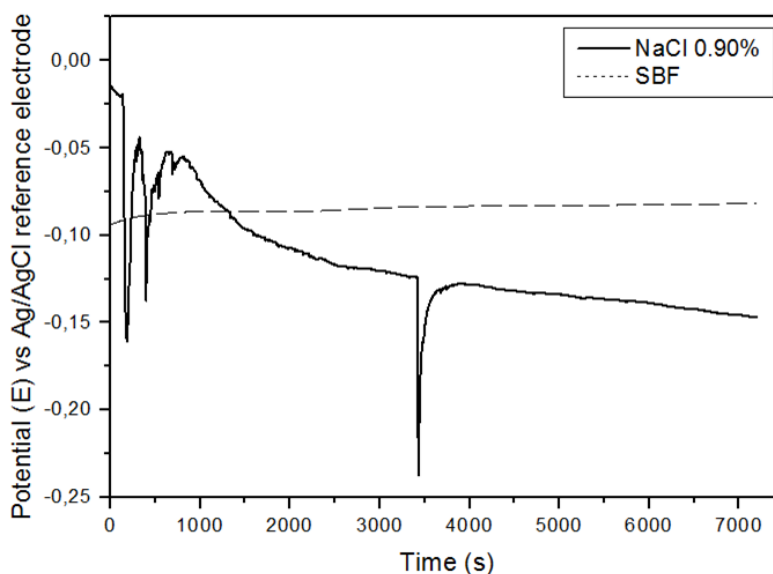


**Figure 1.** Variation of open circuit potential as function of the immersion time of ISO 5832–1 stainless steel in 0.90% NaCl and SBF solutions.

Figure 1 shows very stable potential values over time obtained using the SBF solution. Using NaCl solution, there were large potential oscillations, typical of localized corrosion. The tendency of potential decreasing with the time immersion indicated corrosive attack of the medium to the passive film, initially present on the steel surface.

The potential stability of the steel in SBF solution indicates that in this medium the passive film was preserved over the duration of the test and the medium was not aggressive enough to cause damage to the oxide layer.

Figure 2 shows the anodic polarization curves obtained potentiodynamically for ISO 5832–1 steel in NaCl and SBF solutions.

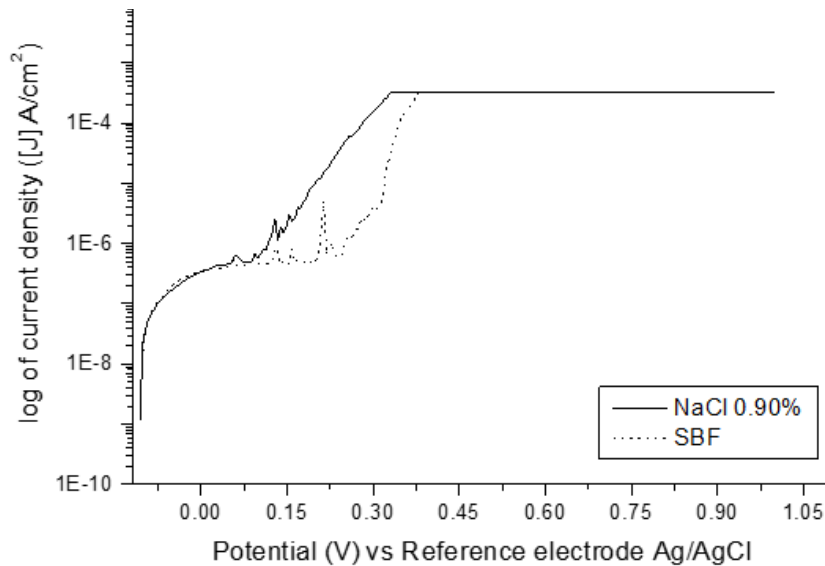


**Figure 2.** Potentiodynamic polarization curves of the ISO 5832–1 stainless steel in NaCl and SBF solutions.

The anodic polarization curves showed typical behaviors of passive materials from open circuit potential to passive film break potential, indicated by the gradual current increase. The passive film breaks potential were observed at potentials of about 0.12 V for NaCl solution, and of 0.25 V for the SBF solution. These results confirm that open circuit potential measurements showed a higher tendency to localized corrosion associated with chloride medium.

The surfaces of the ISO 5832–1 steel samples obtained after electrochemical tests were analyzed by scanning electron microscopy (SEM) to characterize the morphology and sizes of the attacked areas and these are shown in Figures 3 and 4. Surface analysis of these Figures after the polarization test confirmed crevice corrosion on these surfaces. This was explained by the oxygen gradient due to the rod presence on the exposure area, causing crevice corrosion promoted by differential aeration cells.

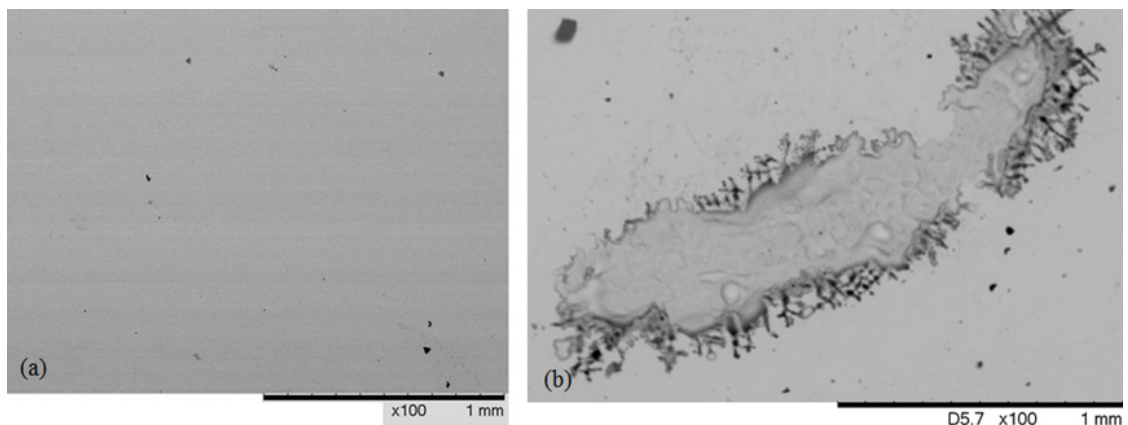


**Figure 3.** Micrographs obtained by SEM: (a) Surface of ISO 5832–1 steel polished before electrochemical testing; (b) Surface of ISO 5832–1 steel showing crevice corrosion after anodic polarization test in 0.90% NaCl.

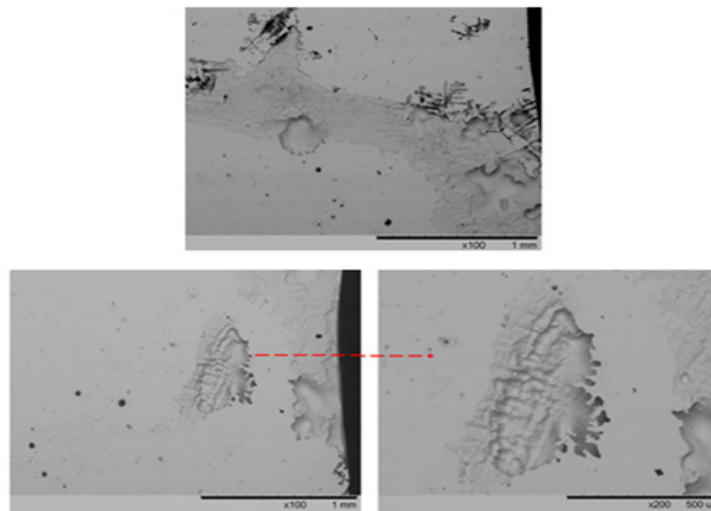


**Figure 4.** Micrographs obtained by SEM of the corroded region on the surface of the polished sample of ISO 5832–1 steel after polarization test in SBF solution showing crevice corrosion.

The comparison of the micrographs of the Figures 3 and 4 shows that the areas attacked by crevice corrosion were higher in the case of NaCl solution than that in SBF solution. These results are in agreement to the Figure 1 and Figure 2 of electrochemical tests.

### Conclusions

The obtained results allowed concluding that the NAA technique can be properly applied in the determination of the chemical elements present in the ISO 5832–1 austenitic stainless steel. Cr, Cu, Mn, Mo and Ni results determined in this alloy are within the specification of this steel. In addition, elements As, Co, V and W that are not shown in the specification of this material were determined.

Corrosion tests have shown that ISO 5832–1 steel presents different behavior between NaCl and SBF solutions. The highest susceptibility to crevice corrosion was verified in NaCl solution, but in SBF solution this alloy showed resistance to this type of attack.

### Acknowledgments

The authors are grateful to São Paulo Research Foundation (FAPESP–BRAZIL), Coordination for the Improvement of Higher Education Personnel (CAPES–BRAZIL), Council for Scientific and Technological Development (CNPq–BRAZIL) and Instituto de Pesquisas Energéticas e Nucleares, (IPEN–CNEN / SP – Projeto Edital 05/2018–Inter Centros) for their financial support. Author L. N. M. Branguin thanks CNPq for the Master's scholarship.

### References

- [1]. Hastings GW. Definitions in biomaterials. In: Progress in Biomedical Engineering. 1st ed. Editor D.F. Williams, Elsevier; Amsterdam, 1987. 72 p.
- [2]. Binyamin G, Shafi BM, Mercy CM. Biomaterials: a primer for surgeons. *Semin Pediatr Surg* 15: 276–283 (2006).
- [3]. Parida P, Behera A, Mishra SC. Classification of biomaterials used in medicine. *Int J Advances Appl* 3: 125–129 (2012).
- [4]. International organization for standardization, Implants for surgery. Metallic materials – Part 1: wrought stainless steel. Switzerland. Reference number ISO5832–1:2007(E) (2007).
- [5]. Dewidar MM, Yoon H, Lim JK. Mechanical properties of metals for biomedical applications using powder metallurgy process: a review. *Met Mater Int* 12: 193–206 (2006).
- [6]. Asri RIM, Harun WSW, Samykano M, Lah NAC, Ghani SAC, Tarlochan F, Raza MR. Corrosion and surface modification on biocompatible metals: a review. *Mater Sci Eng C* 77: 1261–1274 (2017).

- [7]. Sipola T, Alatarvas T, Fabritius T, Peramaki P. Determination of alloying and impurity elements from matrix and inclusions from a process sample of a double stabilized stainless steel. *ISIJ Int* 56: 1445–1451 (2016).
- [8]. Yonga C. ICP–AES determination of 15 kind of impurity elements in the vanadium–aluminum alloy. *Procedia Eng* 24: 447–453 (2011).
- [9]. Acharya R, Kolay S, Reddy AVR. Determination of nickel in finished product alloys by instrumental neutron activation analysis and spectrophotometry. *J Radioanal Nucl Chem* 294: 309–313 (2012).
- [10]. Saiki M, Rogero SO, Costa I, Correa OV, Higa OZ. Characterization of ear piercing studs and their corrosion products by neutron activation analysis. *J Radioanal Nucl Chem* 248: 133–136 (2001).
- [11]. Cincu E, Manea I, Manu V, Barbos D, Sima O, Gustavsson I, Vermaercke P, Vajda N, Molnar Z, Polowska–Motrenko H. Comparative performance of INAA and other spectroscopy techniques in the elemental analysis of stainless steel materials. *J Radioanal Nucl Chem* 274: 199–205 (2007).
- [12]. Shinde AD, Acharya R, Reddy AVR. Analysis of zirconium oxides by relative and internal monostandard neutron activation analysis methods. *Nucl Eng Technol* 49: 562–568 (2017).
- [13]. Cincu E, Cracuyn L, Manea–Grigore I, Cazan IL, Manu V, Barbos D, Cocis A. Application of the INAA technique for elemental analysis of metallic biomaterials used in dentistry. *Appl Radiat Isot* 67: 2133–2136 (2009).
- [14]. Giordano EJ, Alonso–Falleiros N, Ferreira I, Balancin O. Electrochemical behavior of two austenitic stainless steel biomaterials. *Rev Esc de Minas* 63: 159–166 (2010).
- [15]. Braguin LNM, Costa I, Saiki M. Elemental determination of austenitic stainless steel alloy used as biomaterial by neutron activation analysis, *Proc. International Nuclear Atlantic Conference INAC 2019 Santos, Brazil* (2019).
- [16]. De Soete D, Gijbels R, Hoste J. *Neutron Activation Analysis*. Wiley–Interscience, London (1987).
- [17]. National Institute of Standards and Technology, Certificate of analysis. Standard reference material 363 Chromium–Vanadium Steel (Modified) (2012).
- [18]. British Chemical Standards, Certificate of analysis. BCS/SS No. 467, Austenitic stainless steel (n. d).
- [19]. Kokubo T, Takadama H. How useful is SBF in predicting in vivo bone bioactivity? *Acta Biomater* 27: 2907–2915 (2006).



## Production Of Poly(L-Co-D,L Lactic Acid) Porous Fibers By Electrospinning

NMS. Carvalho<sup>1,2</sup>; BE. Ciocca<sup>1,2</sup>; R. Maciel Filho<sup>1,2</sup>; MF. Passos<sup>2,3</sup>; MR. Wolf Maciel<sup>1</sup>; R. Furlan<sup>4</sup>

\*Corresponding author: e-mail address: [nayaramaysa@gmail.com](mailto:nayaramaysa@gmail.com)

**Abstract:** The production of porous scaffolds has been widely investigated by the scientific community due to its suitability for tissue engineering. Among techniques that allow the fabrication of porous materials, electrospinning is appealing for being robust and versatile. This research investigated the pore formation in poly (L-co-D,L lactic acid) fibers obtained by conventional electrospinning and the influence of chloroform as a single solvent on fiber morphology. Random and highly porous fibers with a mean diameter of  $2.373 \pm 0.564 \mu\text{m}$  were collected. Chloroform affects the fiber morphology, mainly for its fast evaporation and low density of charges. The solvent on the surface evaporates quickly, and the low stretch of the jet does not help the polymer to reorganize over the length of the fiber, forming pores. In conclusion, the low dielectric constant and boiling point of chloroform induce pores formation along the PLDLA fibers.

**Keywords:** Porous scaffold. Nonwoven. PLA. Chloroform.

### Introduction

The fabrication of scaffolds from nanofibers has been widely investigated by scientists. Among all possible structures, porous nonwoven made of micro and nanofibers arouses great interest in the scientific community and technology industry. Pores might be formed between adjacent fibers, the inter-fibers pores, or within a fiber, the intra-pores. In a membrane, the interconnected pores might be classified by the length, where there is macro ( $> 450 \text{ nm}$ ), meso ( $2 - 50 \text{ nm}$ ), and micro-pores ( $< 2 \text{ nm}$ ).<sup>1,2</sup> Designing such anisotropic functional textiles that allow fast penetration of sweat through one direction but prevent its movement in the reverse direction is still a challenging task. In this regard, fabrication of a novel Janus membrane with multi-scaled interconnected inter- and intra-fiber pores for enhanced directional moisture transport designed by a rational combination of superhydrophilic hydrolyzed porous polyacrylonitrile (HPPAN

An appeal of intra-pores in nonwovens is its capacity to mimic the extracellular matrix and its high surface area, which favors cell attachment and proliferation over the scaffold. Meanwhile, the existence of intra-pores is a key factor for the material's performance towards wicking and permeability.<sup>1,3,4</sup> applied voltage, spinning distance

Several techniques allow the production of porous structures production such as electrospinning, electrospraying, chemical vapor deposition, and nanoimprinting, among others. Nevertheless, electrospinning has an appeal for being a robust and versatile technique. By changing the polymer solution properties and the several processing variables, a range of nanofibers morphologies may be assembled. The use of electrospinning to obtain artificial materials with different porous hierarchies is also possible. However, mastering the design and fabrication of porous materials according to the demand of the application desired,

containing intra or inter-fiber pores, with micro, meso, and micro-pores, is still a challenge.<sup>4</sup>

The capacity of processing several types of materials is also an advantage of electrospinning. Natural and synthetic polymers processed with this biomedical technology have been successfully reported, as for the use of collagen-gel nanofibers for endothelial cell guidance<sup>5</sup>, for bone critical-sized defects repairing with poly ( $\mu$ -caprolactone) and poly (rotaxane)<sup>6</sup>, for the construction of tubular tissue of poly(trimethylene carbonate-co-(L)-lactide)<sup>7</sup> ISBN:"1742-7061", "ISSN": "1878-7568", "PMID": "23416575", "abstract": "The growth of suitable tissue to replace natural blood vessels requires a degradable scaffold material that is processable into porous structures with appropriate mechanical and cell growth properties. This study investigates the fabrication of degradable, crosslinkable prepolymers of l-lactide-co-trimethylene carbonate into porous scaffolds by electrospinning. After crosslinking by  $\mu$ -radiation, dimensionally stable scaffolds were obtained with up to 56% trimethylene carbonate incorporation. The fibrous mats showed Young's moduli closely matching human arteries (0.4-0.8MPa, for produce bone and fibrous tissue with poly(L-co-L,D lactic acid)<sup>8,9</sup>, and many others.

Poly(L-co-D,L lactic acid) (PLDLA) is a remarkable polymer: it is bioabsorbable, biocompatible, have high mechanical stability and resistance, and very good processability. In brief, it has several advantages and high potential to be widely used in medical devices and biological applications.<sup>8,10</sup>

This research aimed to produce poly(L-co-D,L lactic acid) nonwovens with intra and inter-fiber pores for biomedical applications through conventional electrospinning, and to investigate the influence of the solvent on the formation of intra-fiber pores.

<sup>1</sup> School of Chemical Engineering, University of Campinas (UNICAMP), Campinas, SP, Brazil.

<sup>2</sup> National Institute of Biofabrication, School of Chemical Engineering, University of Campinas (UNICAMP), Campinas, Brazil.

<sup>3</sup> School of Biotechnology, Biological Sciences Institute, University of Pará (UFPA), Belém, PA, Brazil.

<sup>4</sup> Department of Physics and Electronics, University of Puerto Rico at Humacao (UPRH), Puerto Rico, USA.

## Methods

### Preparation of PLDLA solutions

The polymer used was poly(L-co-D,L-lactic acid) (Purasorb PLDL 7038), obtained from Corbion (USA), and the solvent used was chloroform 99,8%, from Acros (USA). The polymeric solutions were prepared using chloroform as a single solvent, and the polymeric concentration was 5 % w/v, determined in previous tests. The solvent was added to the polymer and it was magnetically stirred overnight at room temperature. The solutions were used shortly after preparation.

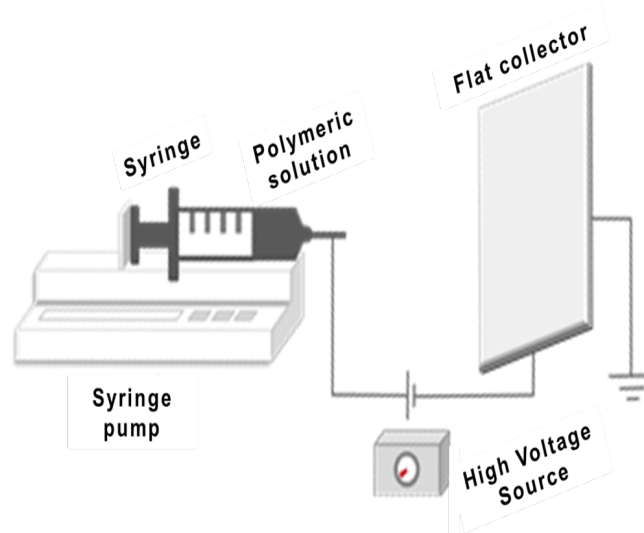


**Figure 1.** Schematic diagram of the conventional electrospinning set up in a horizontal plane.

### Electrospinning process

The solution was transferred to a 20 mL plastic syringe, attached to a metallic flat-end needle (22 G). It was used quickly and for a short time to prevent degradation of the syringe by chloroform. Conventional electrospinning was performed and the fibers were collected in a grounded, static, and flat silicon plate (Figure 1).

The electrospinning parameters were set according to previous tests. The work distance (space between the collector and the needle tip) was 20 cm, the polymer solution flow rate was kept constant at 1.0 mL/h by a syringe pump (Fisher Scientific, USA), and the power applied in the needle (the positive pole) was 15 kV by a high voltage source (Gamma, USA). Samples were produced in triplicate, at room temperature and atmosphere conditions.

### Scanning electron microscopy (SEM)

The fibers collected on silicon were coated with a thin layer of platinum by plasma metallization (Hummer® 6.2 sputtering system, Anatech LTD, USA). Afterward, the morphology of the fibers was observed in a JEOL JSM-6010 Plus scanning electronic microscopy (JEOL Ltd., Tokyo, Japan).

The images taken were analyzed with the software Image J (Image Processing and Analysis in Java, National Institutes of Health, Bethesda, MD) for measuring the diameter of the fibers. The software Action® (Estatcamp, São Carlos, SP) was used to statistical analysis, as descriptive statistics, normality test (Anderson – Darling), and a normalized histogram.

### Fourier transform infrared (FTIR) spectroscopy

FTIR spectroscopy is a powerful non-destructive method for material identification and a well-established tool in polymer analysis (Kazarian & Chan, 2016). The chemical structure of pure PLDLA, pure chloroform, polymeric solution, and fibers was verified using a Spectrum 100 FTIR spectrometer (Perkin Elmer, Billerica, MA, USA). All materials were scanned from 650  $\text{cm}^{-1}$  to 4000  $\text{cm}^{-1}$ , and its transmittance (%) was measured.

## Results and discussion

The experiment intended to obtain porous fibers of PLDLA and discuss the effect of chloroform on membrane and fiber morphology and topography. Chloroform is a nonpolar solvent with low dielectric constant (4.80), low electrical conductivity ( $1.0\text{E}-04 \mu\text{S cm}^{-1}$ ), and highly volatile (boiling point of 61°C).<sup>11</sup>the productivity, and the morphology of nanofibers. In this study, poly lactic acid (PLA) Its properties have caused some difficulties during the electrospinning process. The low boiling point leads to early solvent evaporation, which has promoted frequent needle clog. The low conductivity, which means reduced charges density in the solution, allowed fibers scattering and low yield (the fibers were sparsely collected in the silicon plate). Despite the adversities, it was possible to collect PLDLA fibers on the silicon plate.

The SEM images obtained (Figure 2) shows continuous fibers, without beads and merged areas, and with a rough surface. The production of a nonwoven with intra-fibers pores was achieved. The absence of beads suggests that the polymer concentration used was adequate since the balance between solution viscosity, surface tension, and electrostatic repulsion resulted in a continuous jet.<sup>11,12</sup> and the formation mechanism of the membranes was determined in this study. The PLA fibrous morphology, including the fiber diameter, bead size, number of beads, and surface structure of the beads, could be closely controlled by regulating the solvent compositions and the concentrations of the PLA solutions. The filtration performance, which was evaluated by measuring the penetration of sodium chloride (NaCl)

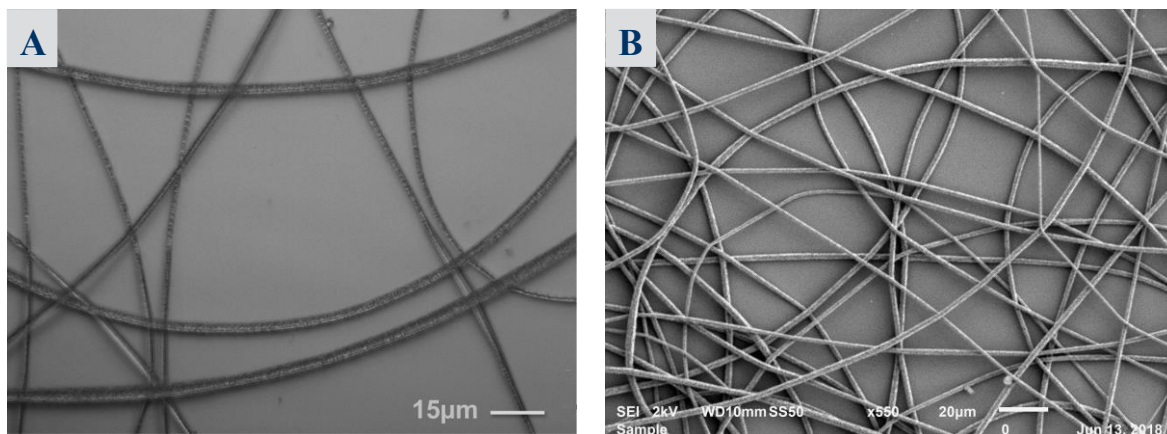


**Figure 2.** Morphology of the electrospun PLA fibers, taken with (A) optical microscope with scale bar of 15 μ, and (B) SEM image with 550 x magnification and scale bar of 20 μ.

According to descriptive statistics of the fiber diameters data (N=50), the mean diameter is  $2.373 \pm 0.564 \mu\text{m}$ , higher than the values reported for electrospun PLDLA with other solvents, as the beaded fibers measuring  $0,352 \pm 0,197 \mu\text{m}$ , produced with N,N-dimethylformamide.<sup>10</sup> However, the fibers were a lot smaller than PLDLA fibers obtained by other methods, as polymerization and condensation:  $110 \pm 10 \mu\text{m}$ .<sup>9</sup> The fiber diameter matters because it is inversely proportional to the number of pores and porosity.<sup>13</sup>

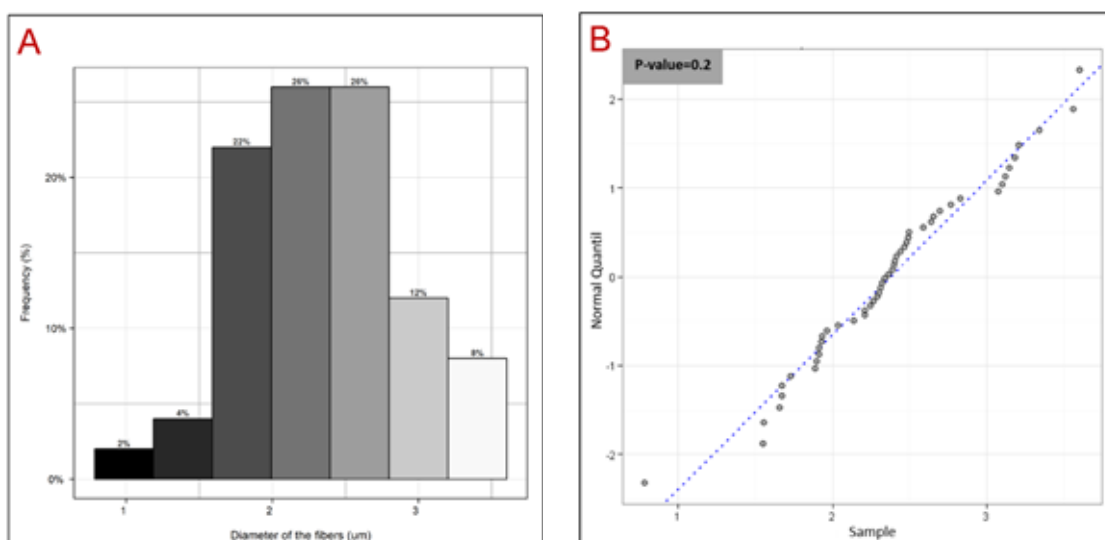


**Figure 3.** (A) Histogram and (B) normal probability plot of fibers diameter measurements.

The wide distribution of the histogram (A – Figure 3), and the large standard deviation (about 20% of the mean diameter) suggest that the forces on the jet were not strong enough to elongate the fiber and reduce the diameter variation as well as the mean diameter. Despite that, the shape of the histogram suggests that the measurements of the diameter have a Gaussian distribution, with a narrow peak. It indicates that the sample has homogeneous morphology and stability during

the process.<sup>14</sup> The normality test (Anderson – Darling) confirmed the normality of the population at 95% of confidence, with a P-value of 0,1971 (higher than 0,05), and by the normal probability plot (B – Figure 3), where the empirical data are positioned over the values of a standard quantile of a normal distribution (dotted blue line).

The central aspect of the fibers is the irregular surface and intra-fiber porosity, easily observed in the SEM images (Figure 4). Mo et al.<sup>15</sup> obtained porous nonwoven with polymethacrylate, and the surface of the fibers was irregular and porous as well. Their tests proved that this fiber aspect leads to a high capacity to absorb oleophilic material. As this characteristic persisted in the PLDLA fibers, this material might be used as an intermediate layer between different phases and promote better integration between it.

The use of a nonsolvent is appropriate to obtain highly porous fibers because it promotes phase-separation (solvent and polymer).<sup>16</sup> However, as chloroform is indeed a good solvent for PLDLA, this mechanism does not explain the pores in PLDLA surface. In this way, phase-separation is not the cause of pore formation.

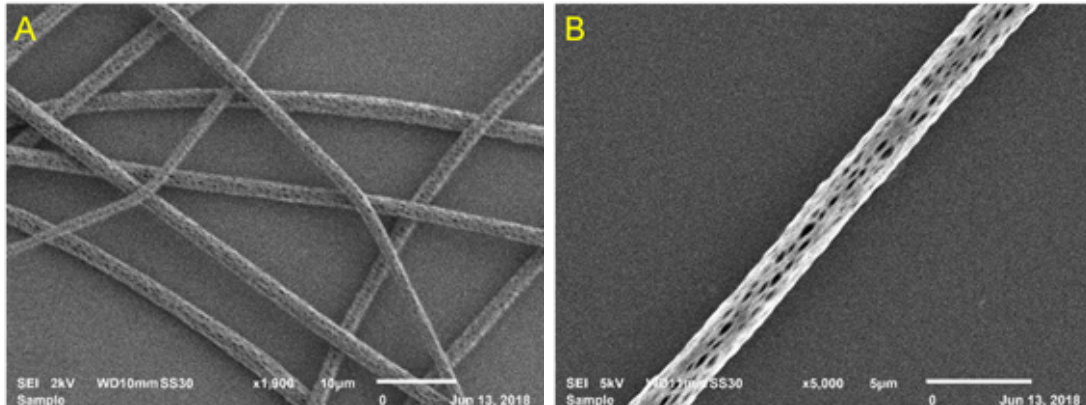


**Figure 4.** SEM images of porous fibers obtained by electrospinning of PLA in chloroform at 5% w/v concentration at (A) 1900 x magnification, with scale bar of 10  $\mu$ , and (B) 5000 x magnification, with scale bar of 5  $\mu$ .

The low boiling point of chloroform suggests that the pores on the fiber were formed for the fast evaporation of the solvent. In addition to it, the polymeric solution with pure chloroform has low charges density, and the jet stretch promoted by the electrical field is weak. Thus, the chloroform evaporation results in gaps in the jet, and the polymeric chains do not redistribute along it because the electrical field is low. As a result, the polymeric chains do not redistribute itself and fulfill the gaps generated by the solvent evaporation, and a porous fiber is formed.

When the boiling point of the solvent is low, but the electrical conductivity is high, this phenomenon does not occur and the fibers present homogeneous and smooth surface, as for PLLA in pure acetone, observed by Casasola et al.<sup>11</sup> This fact corroborates the idea that the specific chloroform properties, low boiling point allied to low conductivity, promote the formation of porous fibers with a large diameter when compared with other electrospun PLDLA fibers.

Another mechanism for pores formation in the fibers is due to high humidity during the electrospinning. As there is no information on relative humidity, it is not possible to assure that the pores and roughness of the fiber surface were aggravated by it, although it is possible.<sup>17</sup>

## Conclusion

The electrospinning of poly(L-co-D,L acid lactic) was conducted using chloroform as a solvent to obtain porous fibers for medical device production. Chloroform changed the morphology of the fibers, highlighting its low boiling point and dielectric constant. Its fast evaporation induced the formation of the pores along the fibers, while the low dielectric constant of the chloroform prevented the polymeric redistribution along the jet in a way that maintains the pores. The low charges density also caused a wide diameter distribution and thicker fibers compared to previously reported PLDLA fibers produced with other solvents. In this way, this research contributed to improve knowledge of the events that promote inter and intra-fiber pore formation for PLDLA.

## Acknowledgments

We acknowledge the Sao Paulo Research Foundation (FAPESP – grant #2015/20630–4), National Council for the Improvement of Higher Education (CAPES – n°33003017034P8), Red Macro Universidades de América Latina y el Caribe and National Institute of Science and Technology in Biofabrication (BIOFABRIS, Brazil).

## References

- [1]. Yan, W. et al. Multi-scaled interconnected inter- and intra-fiber porous janus membranes for enhanced directional moisture transport. *J. Colloid Interface Sci.* 565, 426–435 (2020).
- [2]. Yang, X.-Y. et al. Hierarchically porous materials: synthesis strategies and structure design. *Chem. Soc. Rev.* 46, 481–558 (2017).
- [3]. Katsogiannis, K. A. G., Vladislavljević, G. T. & Georgiadou, S. Porous electrospun polycaprolactone fibers: Effect of process parameters. *J. Polym. Sci. Part B Polym. Phys.* 54, 1878–1888 (2016).
- [4]. Jiang, T., Carbone, E. J., Lo, K. W.-H. & Laurencin, C. T. Electrospinning of polymer nanofibers for tissue regeneration. *Prog. Polym. Sci.* 46, 1–24 (2015).
- [5]. Laco, F., Grant, M. H. & Black, R. A. Collagen-nanofiber hydrogel composites promote contact guidance of human lymphatic microvascular endothelial cells and directed capillary tube formation. *J. Biomed. Mater. Res. Part A* 101A, 1787–1799 (2013).
- [6]. Salles, T. H. C. et al. In vitro and in vivo evaluation of electrospun membranes of poly ( $\mu$ -caprolactone) and poly (ro-taxane). *Mater. Sci. Eng. C* 77, 912–919 (2017).
- [7]. Dargaville, B. L. et al. Electrospinning and crosslinking of low-molecular-weight poly(trimethylene carbonate-co-(L)-lactide) as an elastomeric scaffold for vascular engineering. *Acta Biomater.* 9, 6885–97 (2013).
- [8]. Más, B. A. et al. Biological Evaluation of PLDLA Polymer Synthesized as Construct on Bone Tissue Engineering Application. *Mater. Res.* 19, 300–307 (2016).
- [9]. Länsman, S. et al. Poly-L/D-lactide (PLDLA) 96/4 fibrous implants: Histological evaluation in the subcutis of experimental design. *J. Craniofac. Surg.* 17, 1121–1128 (2006).
- [10]. Carvalho, N. M. S. et al. Production of nanofibers from polylactic acid by electrospinning using N,N-Dimethylformamide as a solvent. in *23 Congresso Brasileiro de Engenharia e Ciência dos Materiais* (2018).
- [11]. Casasola, R., Thomas, N. L., Trybala, A. & Georgiadou, S. Electrospun poly lactic acid (PLA) fibres: Effect of different solvent systems on fibre morphology and diameter. *Polymer (Guildf)*. 55, 4728–4737 (2014).
- [12]. Wang, Z., Zhao, C. & Pan, Z. Porous bead-on-string poly(lactic acid) fibrous membranes for air filtration. *J. Colloid Interface Sci.* 441, 121–129 (2015).
- [13]. Ziabari, M., Mottaghitalab, V. & Haghi, A. K. Evaluation of electrospun nanofiber pore structure parameters. *Korean J. Chem. Eng.* 25, 923–932 (2008).
- [14]. Pereira Rodrigues, I. C. et al. Polyurethane fibrous membranes tailored by rotary jet spinning for tissue engineering applications. *J. Appl. Polym. Sci.* 137, 48455 (2020).
- [15]. Mo, J., Xu, N., Xiao, C., Han, X. & Liu, Y. Structure and property of electrospun fibrous mat based on polymethacrylate. *J. Mater. Sci.* 49, 4816–4824 (2014).
- [16]. Qi, Z., Yu, H., Chen, Y. & Zhu, M. Highly porous fibers prepared by electrospinning a ternary system of nonsolvent/solvent/poly(l-lactic acid). *Mater. Lett.* 63, 415–418 (2009).
- [17]. Kopp, A. et al. Effect of process parameters on additive-free electrospinning of regenerated silk fibroin nonwovens. *Bioact. Mater.* 5, 241–252 (2020).



## Systematic review: the use of vaginal mold in current vaginoplasty surgeries – techniques and materials

JS. Ávila\*<sup>1</sup>; LC. Mendes<sup>1</sup>

\*Corresponding author: e-mail address: [jessicavilaftp@hotmail.com](mailto:jessicavilaftp@hotmail.com)

**Abstract:** This paper presents a study of the techniques and materials used in vaginoplasty surgeries performed around the world. It consists of a systematic review that covered the identification, selection and critique of primary studies of topics involving the use of vaginal molds in surgeries for different patients: women with Mayer–Rokitansky syndrome; and transgender patients who underwent sex reassignment surgery (CRS), that is, patients with gender dysphoria. The researches made in the chosen databases, after applying the criteria of inclusion and exclusion of articles, resulted in 19 publications, which represented the basis of the construction of this work. It also focuses on the description of the technologies, materials and methods used in the manufacture of vaginal molds used in surgery. In all studies, the molds have the function of maintaining the structure of the neovagina, thus avoiding vaginal stenosis, besides fixing the material used as a graft in the new cavity, covering it, favoring epithelization.

**Keywords:** Vaginoplasty. Bioaterials. Vaginal mold.

### Introduction

A systematic review is a secondary and retrospective study that brings together several primary studies that address the same issue to be discussed and evaluated, in this case a vaginoplasty surgery, which uses, in the postoperative period, a vaginal mold, formed by a base covered by graft. The work involved the study of techniques and materials applied in surgery and presents five main applications of vaginal molds.

As described previously, the two main groups of patients who undergo vaginoplasty surgery, with a need to use vaginal mold are: the patient who presented a Mayer–Rokitansky syndrome; and sex reassignment operation patients, that is, transgender people.

In both groups, it is sought the creation of a neovaginal cavity, which can be made by different techniques. After the vaginal canal is constructed, it is necessary to use a mold to keep the width and depth of the vagina intact, and also to fix the material used as a graft that will cover the created cavity, which will facilitate epithelization.

### Mayer–Rokitansky–Kuster–Hauser syndrome

The Mayer–Rokitansky–Kuster–Hauser syndrome (MRKH), better known as Rokitansky's syndrome, is a disorder that occurs in women and mainly affects the reproductive system. It represents a malformation characterized by complete or partial agenesis of the vagina and uterus, causing them to be underdeveloped or absent. This syndrome represents the second most common cause of primary amenorrhea, a gynecologic cause where the first menstruation does not occur (menarche)<sup>1,2</sup>.

There are two types of MRKH syndrome, being types 1 and 2. Type 1 is characterized by an isolated absence of the proximal two-thirds of the vaginal cavity, while type 2 is marked by other malformations, including vertebral, cardiac and urological abnormalities, for example<sup>1</sup>.

Individuals with this syndrome have a normal karyotype, regular ovarian hormone function, and external genitalia. Thus, the development

of secondary sexual characteristics and adolescent progress is normal. However, women affected by the syndrome generally do not have menstrual periods due to the absent uterus, and although the fact that women with this condition can not withstand pregnancy, they can have children through assisted reproduction<sup>1,2</sup>

The treatment goal, whether done conservatively or surgically, is to provide the patient with a suitable passageway for penetration, facilitating a satisfactory sexual intercourse. The functional neovagina created, will allow the patient to achieve physical and psychological balance<sup>3</sup>.

### Gender Dysphoria

Patients with gender dysphoria (transgender) present persistent discomfort with the sex imposed at birth. Because of a sense of inadequacy in the social role of this genre, these people have an unalterable conviction that they were born in the wrong body, causing great psychological distress from early youth.

According to the International Classification of Diseases, revision 10 (ICD–10), the following three criteria must be detected before an individual can be diagnosed with gender dysphoria: (I) the person has the desire to live and be accepted as a member of the opposite sex; (II) this desire is usually accompanied by a sensation of discomfort or inappropriateness of the anatomical sex; and (III) the desire to undergo hormonal surgery and / or treatment to make your body as congruent as possible with the preferred sex, causing the primary and secondary characteristics of the sex to be lost in order to gain those of the opposite sex<sup>4,6</sup>.

When the diagnosis and indication for surgery are confirmed, the individual initiates hormone therapy, developing, as a consequence, relatively acceptable breast tissue. Thus, early hormonal treatment may turn procedures, such as maxillofacial surgery, unnecessary or less invasive in these patients. In this way, it is believed that the best treatment is either hormonal therapy or gender shaping surgery that transitions the

<sup>1</sup>Dep. De Engenharia Elétrica, Universidade Federal de Uberlândia, Uberlândia (MG), Brasil.

individual into the desired gender, playing a crucial role in relieving their psychological discomfort<sup>4</sup>.

For each patient, the psychological eligibility, before performing the surgery, is evaluated by qualified professionals, properly trained in mental health and experienced in gender dysphoria evaluation. Such assessment is done through several counseling sessions, according to the standards of transgender health care<sup>5</sup>.

The goals of the procedure, which can be done only by surgical intervention, are: to create a female vulva; a deep vaginal cavity and wide enough to facilitate penetration; a sensitive clitoris; and the majus and minus labiums, with the fewest surgical complications<sup>5</sup>.

### Objectives

As the amount of scientific information is increasing regarding the use of a vaginal mold in surgeries for the formation of neovaginas, it is necessary to optimize this information, so that will be better used. The amount of people who depend on this technology increases every day, being indispensable the development of studies and research related to the subject.

Among all the articles studied, there is a lot of information about the techniques used, and very few about the mold itself. The lack of research in this area is evident, and in return, there is a huge demand of patients who depend on this technology.

Thus, a systematic review was developed bringing together several primary studies, based on the same theme, described above. The objective is to identify materials and methods used in surgeries, specifically in the case of mold, in order to obtain an evaluation of the eligibility, safety and effectiveness of the entire process.

### Materials and methods

The first step of all scientific work consisting of a systematic review is the elaboration of a question that is sufficiently clear, objective and directed to the research topic to be developed. Thus, its elaboration was allowed using a tool designated by the acronym PICO. In this, the letters correspond to: "P" the population, "I" the intervention, "C" the comparison, and "O" the outcome. The strategy for preparing the PICO question is used to identify what the question should specify.

In this way, the defined question was: "In patients with Mayer–Rokitansky syndrome and / or patients with gender dysphoria, where both groups undergo vaginoplasty surgery, the mold used to maintain the vaginal cavity open made by a relatively rigid material with skin graft compared to a flexible and biocompatible material, results in better post–surgical results? ".

From this, research was done to search for scientific articles in BIREME, PUBMED, PORTAL CAPES, LILACS and CLINICAL TRIALS databases. The keywords were: vaginal mold, vaginoplasty, Mayer–Rokitansky syndrome, sex reassignment surgery and transgenitalization.

The researches in the databases were written without crossing the keywords, and in each one, all articles were selected and included in a spreadsheet made in Excel. It is important to note that all keywords were researched in three different languages: Portuguese, English, and Spanish.

The first exclusion criterion applied was the repetition of articles. After excluding all repeated articles, a second criterion was proposed, excluding all articles that did not fit the theme, with the exclusion of the majority. Then there was a third criterion, which excluded articles with incomplete texts, and also did not contribute significantly to the research.

Figure 1 shows the tool used for the identification, selection, eligibility, and inclusion of articles. The study resulted in an initial result of 1,121 articles, and after the application of all the exclusion criteria, this number reduced to 19. From then on the articles were studied and evaluated.

### DEVELOPMENT

#### Vaginoplasty

Vaginoplasty is a surgical procedure characterized by the creation of an artificial vaginal cavity, applied in cases of congenital absence of the vagina due to vaginal agenesis, or in cases of operation for sexual reassignment, where there is no vaginal cavity<sup>1</sup>. Thus, vaginoplasty has a considerably positive impact on the quality of life of these patients<sup>5</sup>.

The main method to construct the vaginal cavity in a patient with Rokitansky's syndrome is by dissecting tissues between the rectum and the bladder. For trans patients, this process is also performed, but mainly by the penile inversion method, representing the final phase of the process of gender conformation. Both procedures are done surgically, although there are also non–surgical techniques for the creation of a neovagina in patients with the described syndrome.

Several complications can be verified in these procedures, the main ones being:

Vaginal stenosis, which represents the most common complication that can occur. It is characterized by significant closure or narrowing of the neovagina, associated with misuse or abandonment of the mold in the postoperative period. If the patient has a long and correct postoperative period of dilatation, neovagina will not be closed nor narrowed in terms of diameter and length<sup>1</sup>;

Fistulas formation, which represent the most serious complication in such procedure. If fistula formation occurs during

the operation, the original procedure should be abandoned and treatment to close the fistula should be instituted first<sup>1</sup>. The fistula represents the formation of a canal that abnormally communicates two internal organs or an internal organ with the surface of the body;

Rectal or urethral lesions, characterized by being common intraoperative complications due to the occurrence of damage to the rectum and urethra, respectively<sup>5</sup>;

Infections in general, which may be manifested in the short-term postoperative period<sup>5</sup>;

Long resting time and very intense pain in the graft donor region<sup>5</sup>.

The participation of a multidisciplinary team, with accompaniment of professionals specialized in the approach of the sexual disorders, is fundamental for a good evolution, even before the surgical approach. This is necessary because, since surgery is relatively complex and presents uncomfortable postoperative, there is a very high probability of the patient's resistance to accepting the neovagina as a functional organ<sup>7</sup>.

There are several non-surgical and surgical treatment techniques described in the literature for the correction of vaginal agenesis<sup>3</sup>, as well as several surgical treatment techniques for CRS. However, this work will mention two techniques applied in patients presenting with Rokitansky's syndrome, and a technique applied in trans patients.

Treatment options, which may consist of surgical and non-surgical vaginoplasty, depend on several factors, including patient preparation, preference and expectations, and certainly the surgeon's experience<sup>8</sup>.

### **Techniques applied in patients with Rokitansky's syndrome**

#### **Frank Method**

Frank's method, which consists of a non-surgical procedure, uses manual physiotherapy techniques performed by the women affected by the syndrome to form the vaginal cavity. It is a technique that requires time and motivation of the patient, which should be reinforced by the companion who supervises her case<sup>1</sup>. This method is usually applied in women who already have a certain vaginal length before initiating treatment<sup>9</sup>.

The basis of this approach is graduated dilation of the vaginal cavity, made by means of dilators, which are placed against the vagina and pressed firmly for 15 minutes, twice a day or more frequently. As the ideal length of the cavity is reached, the frequency and the pressure applied to the vagina decrease progressively<sup>1</sup>.

Due to the characteristics of the method, compliance is considered weak in patients with complete absence of the vagina, since these patients suffer much discomfort and abandon treatment with the dilator<sup>1</sup>.

Several studies have shown that women who can not complete the treatment using the Frank method have a lower mean vaginal length at the beginning of treatment than those who completed it<sup>9</sup>.

Although non-surgical techniques for the creation of a neovagina have been reported, medical surgeons prefer the surgical method, since the time interval of the treatment using the Frank method for example is long and can reach up to two years duration<sup>10</sup>.

#### **McIndoe Method**

The McIndoe method, which consists of a surgical procedure, represents the creation of a vagina by the blunt dissection of tissues and structures located between the bladder and the rectum, with a dermal coating used as a graft. This surgical procedure was initially conceived by Abbe and later modified by McIndoe<sup>11</sup>.

The surgical procedure based on this technique follows approximately the following steps:

Firstly, after local anesthesia, the patient is placed in a lithotomy position<sup>11</sup>, that is, placed in the supine position, with the head and shoulders slightly raised, the thighs being well flexed on the abdomen, separated from each other;

The catheterization of the urethra is then performed. Generally a small amount of methylene blue is instilled through the catheter into the bladder in order to detect a possible injury due to dissection performed in the wrong way and can be diagnosed as soon as possible. If the blue colored fluid is aspirated, it means that the direction of dissection in relation to the bladder is incorrect<sup>1</sup>;

Then the labium minus are separated, and an incision of approximately 0.5 cm is made in the region of the cavity to be formed. So the shear dissection is performed, reaching an ideal vaginal length, usually 10–12 cm<sup>11</sup>;

The space is coated instead by a skin graft removed from the buttocks, thigh or suprapubic region<sup>1</sup>, which is cast on a base, forming a vaginal mold, presenting a bottom surface facing outside, so that it is in contact with the newly created vagina.

Finally, the edges of the labium majus are sutured together to help hold the mold in place during the first postoperative week. After seven days the labial sutures and the template are removed, and the cavity is inspected to evaluate the progress of epithelialization, and healing<sup>1</sup>. Generally, the mold is sanitized with physiological saline under pressure;

After the surgical procedure, the patient is still instructed to perform exercises four to six times a day with a dilator to stimulate the dilation of neovagina. Initially, this dilation is considered by the vast majority of patients to be heavy and painful, but over time, it becomes less frequent and difficult. The final result consists of a cavity measuring approximately

10 to 12 cm deep and three fingers wide<sup>1</sup>.

The main disadvantages related to this procedure are: surgical complexity; severe pain at the site of the skin graft; scar due to graft removal; possibility of keloid formation at the donor site; and if the patient does not perform the dilation exercises, the neovagina may contract and cause the canal to close, necessitating a new surgery<sup>8</sup>.

Several modifications of the McIndoe technique have been proposed, especially in relation to the material used as coating of the cavity. The main applications of these materials in vaginoplasty surgery include, in addition to the use of skin grafts: allogeneic amniotic membrane; peritoneal layers; and autologous buccal mucosa.

The use of allogeneic amniotic tissue, which does not originate from the patient itself, brings with it the inherited disadvantage of allograft rejection and the high risk of transmission of infectious diseases. The use of the peritoneum has the disadvantage of requiring the opening of the peritoneal cavity, characterizing another surgical procedure, which should be strongly avoided. The use of autologous buccal mucosa, which means to use the patient's own graft, although it does not leave external scars, presents as disadvantages the morbidity related to removal of the mucosa from the donor site and the need for a relatively long time to reach a functional vagina<sup>1,11</sup>.

## **Techniques applied in patients with gender dysphoria**

### **Penile Inversion Method**

The penile inversion method, which consists of a surgical procedure, represents the creation of a vagina, by the inversion of the penis, where there is the formation of the vulva; vaginal cavity; clitoris; and minus and majus labium<sup>5</sup>.

Since this is an extremely complex procedure, it is necessary that patients be admitted to the intestinal preparation through specific medications, and when they start the surgery, they also receive antibiotic prophylaxis<sup>5</sup>.

The surgical procedure based on this technique follows approximately the following steps:

First, after epidural anesthesia, the patient is placed in a lithotomy position and the surgical area is disinfected<sup>5</sup>;

Then, a catheter is placed in the urethra, and a circumcision is performed at the base of the foreskin. The skin of the penis and the urethra are separated from the cavernous bodies<sup>14</sup>;

The dorsal neurovascular bundle is then also separated from the cavernous bodies, leaving the penile glans and the foreskin vascularized;

Then, the neovaginal space is dissected until a depth of approximately<sup>14</sup> cm is reached. The correct identification of anatomical layers, avoiding lesions in the urethra, prostate, seminal vesicles, sphincter and bladder, is essential<sup>14</sup>;

Then, of a part of the glans of the penis and the foreskin, the neoclitoris and the minus labium are sculpted, respectively. The scrotal skin is excised to define the majus labium<sup>14</sup>;

As in the McIndoe method, the newly formed space is covered by a mold, formed by a base, on which is sewn a skin graft, mainly removed from the abdominal region. The deep surface of the graft is facing outwards so that it is in contact with the wall of the vaginal canal created<sup>11</sup>;

Finally, the edges of the majus labium formed are also sutured together to keep the mold in place for the first seven postoperative days. As in the McIndoe method, after surgery, the patient is instructed to perform exercises with a dilator or vaginal shaper in order to stimulate the dilatation of the formed cavity<sup>14</sup>. For the penile inversion procedure, the main disadvantages are also: surgical complexity, which causes many people to become discouraged to perform it; long postoperative period and with several complaints of pain and complications; the scar that remains in the donor site of the skin graft; and the need for a new surgery in the event of vaginal stenosis, due to a lack of correct use or abandonment of the vaginal mold<sup>14</sup>.

### **Applications of the vaginal molds**

As seen previously, the success of the surgical procedure, in both cases presented, is directly related to the use of the vaginal molds in the postoperative period.

The molds used, whose diameters vary between 2.5 and 3.5 cm, according to the phenotypic characteristics of each patient<sup>12</sup>, can be rigid or malleable. The rigid ones often cause a series of complications, such as: graft loss; fibrosis; contracture; bladder or rectal fistula related to pressure; and, mainly, patient discomfort. Malleable molds, however, reduce the number of these occurrences, but may present other disadvantages, including: instability; assembly complexity; and most important, the lack of commercial availability<sup>13</sup>.

In the sections 2.4.1 to 2.4.5 follow the main types of vaginal molds used both in patients with Rokitansky's syndrome and in patients with gender dysphoria. It is important to note that these applications are described in series reports of cases, that is, performed in several patients.

### **Condom filled with foam covered by amniotic membrane**

In most of the articles selected, there is the report of the use of rubber condoms filled with foam, forming the base of the

vaginal mold, presenting amniotic membrane covering this basis, replacing the skin graft. The human amniotic membrane is characterized as a protective biological tissue, applicable to wounds and burns, as it acts as a facilitator of epithelization. Thus, it is seen as an ideal graft of tissue to cover the vaginal cavity formed by dissection<sup>1</sup>.

However, the amniotic membrane requires extremely precise preoperative screening<sup>11</sup>. Serum from all donors need to be tested for hepatitis B, hepatitis C, AIDS (human immunodeficiency virus – HIV), and syphilis. Thus, the membrane is collected under sterile conditions by some seronegative donor during a cesarean delivery, and can be stored in normal saline at 4°C with crystalline penicillin for up to 72 hours<sup>1</sup>.

At the time of application, the membrane is removed from the saline bath and placed on the foam filled condom, the mesenchymal surface facing outwards to adhere to the surface of the formed vaginal cavity<sup>11</sup>. The long axis of the amniotic membrane is placed parallel to the long axis of the condom, its lateral edges are approximated on each side, and then sewn. The customization of the template to the size of the created vaginal cavity is of paramount importance, so that there is no pressure necrosis. Once dimensioned and constructed properly, the mold is inserted into the neovagina<sup>1</sup>.

After approximately seven days of the surgical operation, the mold removal takes place. At this time, a second amniotic membrane application is performed, and if necessary, after a further seven days, a third application is performed<sup>11</sup>.

As a result of this application, epithelization is considered to be rapid, but the use of allogeneic tissues, such as the amniotic membrane, carries the disadvantage of tissue rejection and the risk of transmission of infectious diseases from donor to recipient. In addition, membranes have been shown to be easily contaminated before or after transplantation<sup>11</sup>.

Several patients had vaginal stenosis, neovagina shortening, rectovaginal fistula, uterus vesicle fistula and excess skin in the vaginal introitus – corrected only after a new surgery. The cases related to the main complications, being stenosis and shortening of the vagina, were due to the incorrect use of the vaginal mold in the postoperative period<sup>7</sup>.

### Vaginal Tissue Cultured In Vitro

Another very frequent application in the studies is the use of a base 2 cm in diameter and 12 cm long, consisting of any material, covered by a condom, and, covering this base, a patient's own autologous vaginal tissue), cultured in vitro, acting as a graft<sup>10</sup>. Thus, only patients with a MRKH syndrome can go through this operation and use a mold that is constituted by this technique, since they usually present the lower third of the vagina or a vaginal vulva, not found in transgender patients.

The procedure performed to obtain this epithelium consists in first performing a biopsy of the vestibule of the vagina of 1cm<sup>2</sup> of thickness<sup>10</sup>.

The biopsy then undergoes a process of enzymatic dissociation and the resulting cells are plated and incubated in a device with chemical solution, consisting of a substance designed for the growth of untransformed cell types, in a serum-free formulation<sup>11</sup>.

After one week, once the cells reach 70–80% confluence, cultures are further sown for an additional eight days in order to obtain a fully differentiated mucosal tissue<sup>10</sup>.

The time interval between biopsy and total mucosal tissue differentiation is approximately two weeks. At the end of cultures, autologous reconstructed vaginal tissues reach about 314 cm<sup>2</sup> and are collected from plaques. They are then washed in PBS (phosphate-saline buffer solution), and mounted on gauze embedded with hyaluronic acid<sup>10,11</sup>.

The cultured tissue is fixed to the base with bilateral points, and the cell layer is placed so that it faces the walls of the newly created cavity, remaining with the patient for five postoperative days. After this, the mold is removed and the vagina examined<sup>10,11</sup>. The patient is instructed to use the vaginal mold during the six successive weeks<sup>10</sup>.

After four months of follow-up, the epithelization from the transplanted tissue was observed throughout the formed neovaginal wall. In addition, no cases of stenosis were reported and sexual intercourse was reported as satisfactory by both partners<sup>10,11</sup>.

From this, it may be noted that the technique appears to offer several advantages. Because the graft is autologous and orthotopic (that is, the cultured tissue comes from a viscera that is in its proper place, being transplanted in the same position as it was)<sup>11</sup> there is a low risk of rejection or infections derived from the donor, besides minimizing the discomfort of the patient and avoiding permanent scars, since this procedure leaves no visible scars in relation to graft removal<sup>10</sup>.

Among the disadvantages is the fact that the procedure using this technique can be performed only in centers that have tissue culture laboratories, such as hospitals with burn units or large reference centers. In addition, because the procedure is performed in two stages, the first one is characterized by the biopsy, and the second by the vaginoplasty itself, the surgery must be planned in association with the laboratory so that the surgical procedure is done only when the tissue is ready<sup>11</sup>.

Finally, as this study reports the first case of application of vaginal tissue grown in vitro in humans (previously tested only in mice), the technique indicates that the use of the vaginal mold is done for a prolonged time, and intercourse is avoided for a relatively long period of time, to prevent the formation of a vaginal septum and other complications<sup>10</sup>. Thus, the use of in vitro cultured vaginal tissue is in its initial application phase, and it is necessary to acquire more experience before drawing definitive conclusions, which justifies a more in-depth study<sup>11</sup>.

### **Cica–Care**

In this application we present a vaginal mold formed by silicone gel sheets (Cica–Care) as the base, covered by skin graft. The silicone gel sheets are commonly found in most hospitals, available in sterile packages.

The vaginal mold is made using a silicone gel adhesive sheet and a 16 French Foley urinary catheter. The sheet, measuring 15cm x 12cm, is split in half to make two strips in order to be wrapped around the Foley catheter. No suture is required to adhere the gel sheets to the catheter because of its self–adhesive property<sup>15</sup>.

The complete silicone mold is approximately 6.5 cm long and 2.5 cm in diameter, and can expand after inflation of the catheter until they reach an average of 3.0 cm in diameter<sup>15</sup>.

The skin graft is then harvested and wound around the base, with the inner surface facing outwardly, to adhere to the formed vaginal cavity, in the same manner as in previous applications. The margins of the graft are then sutured so that it is stabilized around the base of the mold<sup>15</sup>.

With the catheter balloon deflated, the vaginal mold is inserted into the neovagine. The balloon is then inflated, enlarging the diameter of the mold, and the labium majus are sutured to prevent involuntary displacement of the balloon. Five days after the surgical procedure, the catheter is again deflated and the vaginal mold is removed<sup>15</sup>.

For this application, the neovagina was satisfactorily rebuilt, but there were many reports of severe pain at the graft donor site. The vaginal mold was reused as a dilator for 6 to 10 months to prevent contraction of the cavity<sup>15</sup>.

Because Cica–Care sheets have smooth gel consistency, they provide comfort and wide applicability to irregular three–dimensional defects. Therefore, the length and diameter of the mold can be easily adjusted according to the selection of the desired size of the sheet, or by changing the number of wraps around the Foley catheter. Moreover, due to the durability of the silicone gel sheet, it can be reused as a postoperative dilator, supporting repetitive sterilization<sup>15</sup>.

However, this is a method that uses skin graft, and therefore, presents great rejection of patients in performing it. The intense pain reported by the patients at the graft donor site is the main reason for their withdrawal from the surgery design<sup>15</sup>.

### **Mold made of porous plastic laboratory centrifuge tube**

A fourth highly successful application in vaginoplasty surgeries is the use of a rigid, disposable porous base made of a plastic centrifuge tube with a conical bottom (approximately 50 ml). This base is covered by skin graft, removed from a donor site.

In the plastic tube, easily found in hospitals and laboratories, several holes are made, traversing all its extension, with the function of storing the fluids originated from the neovagina, after the procedure. The bottom of the tube has an opening, through which gauze is placed inside, used to care for the wound. In this way, the gauze allows the absorption of the fluid discharge, allowing a quick and easy cleaning in the dressing changes<sup>16</sup>.

On this basis, formed by the tube and gauze in its interior, the skin graft is sewn, constituting the vaginal mold. It is then inserted into the formed vaginal cavity, suturing the bottom of the tube into the labium majus in order to hold the mold firmly in place<sup>16</sup>.

This application presents as advantages: the use of a simple base, made of a plastic tube, readily available; possibility of carrying out the frequent exchange of gases located inside the tube, which absorb the fluids from the neovagina; and the possibility of using a vaginal shower to clean the mold in case of local infection<sup>16</sup>.

However, several complications have also been reported, such as: vaginal stenosis; fistula formation; pain in the donor site of the graft; infection; traumatic devascularization; and accumulation of fluid under the graft due to poor drainage<sup>16</sup>.

As the mold is formed of a rigid material, with no possibility of personalizing it to the patient, it becomes practically impossible to minimize the complications caused by its non–ideal size, both in diameter and length. In addition, it is a very painful technique due to the use of skin graft<sup>16</sup>.

### **Interceed**

Summing up, the last application presented in this work consists of a vaginal mold made of any material as base, covered by an Interceed sheet, an absorbable adhesion barrier, used with graft.

Interceed is a whitish, regenerated cellulose tissue that has the objective of reducing the risk of adhesions by creating a gelatinous layer between the surfaces involved in surgical procedures<sup>11</sup>, being an absorbable herbal product that provides a matrix for aggregation of platelets. Oxidized cellulose acts as a protective coating on the neovaginal surface to allow tissue from the vaginal cavity to be epithelialized, since cells in the dissected space between the rectum and bladder have pluripotent potential for tissue differentiation<sup>17</sup>.

For construction of the application, the Interceed sheet is wrapped around the base of the mold, and then the edges of the sheet are sewn so that it does not come off. The product is then inserted into the neovagina, where it remains for about three days. After removal of the mold, the vagina is washed with saline solution and the neovaginal cavity is examined. At this point, it is expected that the oxidized cellulose has been completely absorbed. Patients are instructed on how to use

the vaginal mold, until frequent sexual intercourse begins<sup>11</sup>.

The result of biopsies made long after the procedure identified complete epithelization after five months in all samples. However, in most cases the vagina became stenotic at two months post surgery (because the patients did not use the dilator correctly, as seen). In addition, the samples collected by the biopsies were composed of a connective tissue permeated by numerous inflammatory cells. In several cases, traces of oxidized cellulose were also observed, and therefore not fully absorbed by the body<sup>17</sup>.

The vaginal reconstruction with oxidized cellulose seems to be a safe and effective procedure with minimal morbidity and discomfort, besides presenting antibacterial and absorbable properties. This process is generally described as an attractive method, since the procedure of obtaining the graft is not related to an operative procedure; and the material is readily available for use<sup>17</sup>.

However, the Interceed sheet is contraindicated in the presence of ostensive infection, and also does not act as a hemostatic agent and should be used only after rigorous hemostasis, since its properties are inactive in contact with blood, making it difficult to use in general surgeries<sup>17</sup>.

Finally, a systematic review, published in the Cochrane Database of Systematic Reviews, in 2008, compared the results of 16 clinical trials to evaluate the effectiveness of four barrier products in preventing adhesions in women undergoing pelvic surgery: Interceed, Gore–Tex, Seprafilm and fibrin. It was observed that, in most trials, Gore–Tex was more effective than Interceed<sup>18</sup>.

## Results

As mentioned, three exclusion criteria were applied, which were removed due to: presence of duplicates; existence of articles that did not fit the theme; and also the presence of articles that did not specify any information related to the vaginal molds.

In this way, the research initially presented 1,121 articles. After excluding the repeated articles, there were 869. Then, most of the articles were excluded, after the removal of those that did not fit the theme, leaving 153. Eight articles were eliminated because they did not present the complete text. Of the 145 remaining, 126 were excluded because they did not specify any information about the vaginal mold, leaving 19 articles, which represented the basis of this work.

## Discussion

Surgery performed in both cases is characterized by a complex, irreversible procedure, besides being a process that involves psychological difficulties and disorders both for the patient and for others involved.

The main goal of the surgery is to avoid vaginal constriction and get a good sexual function from the vagina. However, among the applications presented, the surgical return mainly occurs for two reasons: due to the incorrect use of the vaginal mold; or because the graft is formed by a material not favorable to the epithelization of the new surface.

One of the most frequent post–surgical problems, the so–called vaginal stenosis is usually caused by the fact that the mold consists of a rigid and not comfortable material, leading to non–compliance with the dilatation protocol of the newly formed canal. This is due to the patient's anxiety related to possible pain during the movement or reinsertion of the mold into the new cavity<sup>19</sup>.

However, the use of a graft material that does not present favorable characteristics to the cavity epithelization, promotes difficulties related to the requirement of a post–surgical period that is much larger than normal.

In this work, applications of rigid molds and others with certain malleability, for example, cica–care were presented. As expected, the rigid molds caused a series of complications, the main one being the discomfort of the patient. On the other hand, the cica–care presented as a mold of low assembly complexity, stable, and mainly, without presenting severe discomfort to the patient in the postoperative period, favoring its correct use, and avoiding the stenosis of the vaginal cavity. However, in the application involving cica–care, skin grafts were used to cover the base of the mold, this being the technique considered as conventional.

This method, which involves the use of skin grafts, presents several negative points, such as: intense pain at the site of the donor site; require the presence of a team of plastic surgeons to prepare the skin graft; require long surgical and hospitalization period; and finally, to present an unfavorable aesthetic result, since the donor site of the graft usually presents a wide and visible scar.

However, the skin graft may be replaced by other types of materials, such as amniotic membrane, in vitro cultured tissue, or also regenerated oxidized cellulose. Grafts composed of biological tissues present complications due to the physiological differences of these substrates, due to the use of allogenic tissue; and non–applicability of autologous tissues in patients with gender dysphoria because they do not have a vaginal vestibule. As oxidized cellulose has inactive properties in contact with blood, making it difficult to apply.

The molds and grafts presented in this study are clearly obtained improvised, without consistent and safe standards.

Untested materials are used for their applicability, characterizing the necessity of a standard product. Condom filled with foam and centrifuge tube are improvised and unsafe examples, used every day in vaginoplasty procedures, as well as skin grafts, which as evidenced, present a diversity of negative points.

Although there are methods that have yielded relatively good (but not ideal) results for both mold and graft, they have not been used together, and thus, nothing can be said about the effectiveness of both used together. In addition, the existence of some material considered ideal for forming a mold or graft has not been proven in any study.

It should always be emphasized that for these procedures, using an appropriate vaginal cast is of paramount importance for successful results. The lack of commercial availability of a mold consisting of a base with greater malleability and that comply with the needs of users, as well as a graft that can bring favorable and supplementary properties to the application, is the main factor for the elaboration of this systematic review.

### **Conclusions**

In recent years, there have been continuous reports on the reconstruction of numerous vaginal cavities with application of several techniques, and the main and most used can be identified in this work.

In a simplified way, it has been seen that the use of vaginal molds, at present, is done in an unstructured way, without conducting a study to identify which would be the best materials destined for this application. There are no comparisons between different techniques, and choosing one procedure over another requires taking into account the advantages and disadvantages of different methodologies.

The constant use of molds made of rigid bases and inadequate grafts, which cause surgical return, was the main motivation for this study.

The elaborated question of the introduction of this work cannot be answered, since none studied reported the use of a vaginal mold made of a flexible and biocompatible material for both the base and the graft. However, it is expected to carry out researches and studies that prove this, since the number of patients who need this technology increases every day.

From the analysis and evaluation of the applications presented, it is evident the necessity to have in the market a standard product, that is produced specifically for the procedure described in the work: the vaginoplasty. It would be very interesting to elaborate a product that would perfectly suit the two groups of patients presented, ending with the improvisation and the use of techniques and materials not tested when its applicability and effectiveness.

### **References**

- [1] R. Chaudhary, V. Dhama, S. Singh, R. Azad, "Vaginoplasty in mayer Rokitansky–Kuster–Hauser syndrome using amnion: a case series," *International Journal of Reproduction, Contraception, Obstetrics and Gynecology*, vol. 5, n. 11, pp. 3832–3839, 2016.
- [2] B. R. Carvalho, et al., "Natural latex (*Hevea brasiliensis*) mold for neovaginoplasty," *Revista Brasileira de Ginecologia e Obstetrícia*, vol. 30, n. 1, pp. 31–35, 2008.
- [3] M. S. Neto, E. C. Baracat, L. M. Ferreira, "Vaginal reconstruction by McIndoe technique with a vaginal expander mold," *International Journal of Gynecology & Obstetrics*, vol. 73, n. 2, pp. 165–167, 2001.
- [4] K. Morcel, V. Lavoué, F. Jaffre, B. J. Paniel, R. Rouzier, "Sexual and functional results after creation of a neovagina in women with Mayer–Rokitansky–Küster–Hauser syndrome: a comparison of nonsurgical and surgical procedures," *European Journal of Obstetrics & Gynecology and Reproductive Biology*, vol. 169, n. 2, pp. 317–320, 2013.
- [5] R. Rossi Neto, F. Hintz, S. Krege, H. Rübber, F. vom Dorp, "Gender reassignment surgery—a 13 year review of surgical outcomes," *International braz j urol*, vol. 38, n. 1, pp. 97–107, 2012.
- [6] L. Zhu, H. Zhou, Z. Sun, W. Lou, J. Lang, "Anatomic and sexual outcomes after vaginoplasty using tissueengineered biomaterial graft in patients with Mayer–Rokitansky–Küster–Hauser syndrome: A new minimally invasive and effective surgery," *The journal of sexual medicine*, vol. 10, n. 6, pp. 1652–1658, 2013.
- [7] S. W. Kim, et al., "Use of a silicone gel sheet vaginal mold in McIndoe vaginoplasty," *Archives of plastic surgery*, vol. 40, n. 5, pp. 652–655, 2013.
- [8] K. J. Yu, et al., "A detachable porous vaginal mold facilitates reconstruction of a modified McIndoe neovagina," *Fertility*

and sterility, vol. 81, n. 2, pp. 435–439, 2004.

[9] J. Dornelas, et al., “Vaginoplasty with oxidized cellulose: anatomical, functional and histological evaluation,” *European Journal of Obstetrics & Gynecology and Reproductive Biology*, vol. 163, n. 2, pp. 204–209, 2012.

[10] S. E. A. Araújo, P. P. P. Caravatto, A. J. B. A. Chang, F. G. C. M. Campos, M. Souza, “Impacto da videocirurgia na prevenção de aderências,” *Revista Brasileira de Coloproctologia*, vol. 26, n. 2, pp. 208–216, 2006.



## Ibuprofen nanocrystals: Production, lyophilization and release profile

P. Severino<sup>1,2,3\*</sup>; T. Almeida<sup>1,2</sup>; T.C. Barbosa<sup>1,2</sup>; C. Rodrigues<sup>4</sup>; MA. Costa<sup>4</sup>; JN. Ferreira<sup>4</sup>; J. Dias-Ferreira<sup>4</sup>; AR. Fernandes<sup>4</sup>; EB. Souto<sup>4</sup>

\*Corresponding author: e-mail address: [pattseverino@gmail.com](mailto:pattseverino@gmail.com)

**Abstract:** Ibuprofen (IBU) is a poorly water-soluble non-steroidal anti-inflammatory drug with proven effectiveness for treating inflammatory, musculoskeletal, and rheumatic disorders. Nanocrystals (NCs) have been proposed as drug delivery systems to improve the solubility and bioavailability of poorly water-soluble compounds. Ibuprofen NCs (IBU-NCs) have been produced by the melt-emulsification method using a combination of Tween<sup>®</sup>80 (1.0%, w/v)/Span<sup>®</sup>80 (0.5%, w/v) as surfactant as these molecules are generally recognized as safe (GRAS) as non-toxic, non-irritating and are of low cost. The obtained main particle size (z-Ave) and polydispersity index (Pdl) were  $159.4 \pm 3.265$  nm and  $0.24 \pm 0.007$ , respectively. Lyophilization slightly increased the mean particle size and Pdl compared to the non-freeze-dried IBU-NCs. The obtained IBU-NCs powders were of white and fine texture. The type and concentration of cryoprotector (trehalose, glucose, sucrose) influenced both the size and the in vitro release profile tested in Franz diffusion cells. Due to the smaller z-Ave, NCs:Trehalose (2:1) of  $170.6 \pm 3.880$  nm ( $0.417 \pm 0.050$ ), NCs:Glucose (3:1) of  $275.3 \pm 8.351$  nm ( $0.144 \pm 0.021$ ) and NCs:Sucrose (4:1) of  $223.3 \pm 10.35$  nm ( $0.402 \pm 0.016$ ) were selected for the in vitro drug release tests. Within the first 6 hours, resuspended lyophilized nanocrystals released between 50–70% of the drug.

**Keywords:** Ibuprofen. Nanocrystals. Melt-Emulsification Methodology. Cryoprotectants. lyophilization.

### Introduction

Non-steroidal anti-inflammatory drugs (NSAIDs) are widely used for their analgesic and antipyretic actions<sup>(1)</sup>. Their mechanism of action concerns non-selective inhibition of the type 1 cyclooxygenase (COX-1) and type 2 cyclooxygenase (COX-2), which is listed as its principal adverse effects by oral ingestion<sup>(2)</sup>.

Among NSAIDs, ibuprofen has been recommended to treat inflammatory, musculoskeletal and rheumatic disorders<sup>(3-5)</sup>. However, the challenge in pharmaceutical development of such drug is due to its high plasma protein binding (90–99%), short plasma half-life (2.2 hours) with rapid urine removal, reaching the peak plasma concentration in just 1–2 hours<sup>(6)</sup>. Also, IBF shows lipophilicity, a high partition coefficient and low bioavailability through the skin<sup>(7)</sup>.

Many approaches have been exploited to overcome the skin barrier for IBF drug delivery. Nanocrystals (NCs) have significant advantages in improving the bioavailability of poorly water-soluble drugs, due to their high solubilization capacity and the possibility to control the delivery rate<sup>(6,8,9)</sup>. NCs are homogeneous, optically transparent, of low viscosity, thermodynamically stable and can be produced without the need of specialized equipment other than to use a few adjuvants<sup>(9)</sup>.

Nanocrystals have emerged as an interesting drug delivery system for clinical usage. It is defined as a nanotechnology-based formulations with a particles size below 1000 nanometers and have a stable performance by adding an appropriate stabilizer such as polymeric steric stabilizers or surfactant in a aqueous medium – nanosuspension<sup>(10,11)</sup>.

These stabilizers have an important role in nanosuspension,

preventing aggregation among nanocrystals due to their high surface energy which contributes to aggregation between them. They are largely used to overcome the bioavailability and dissolution difficulties of using poor water-soluble drugs in traditional pharmaceutical formulations, which is one of the chief challenges that scientists face in drugs formulations<sup>(10,11)</sup>.

The nanoparticle size allows to increase the surface area and, consequently, enhance the dissolution velocity according with the Noyes-Whitney equation, improving kinetic drug performance. Another important characteristic which made nanocrystals a special formulation is each nanoparticle contain 100% of the drug inside and a polymeric or lipid matrix enclose them, thus, considerable drug concentration is transporting to the target cells, enhancing the bioavailability and, consequently, achieving an appropriate drug concentration for the pharmaceutical effect<sup>(9)</sup>.

The aim of this work has been to develop an ibuprofen nanocrystal formulation by melt-emulsification technique, and evaluate the effect of lyophilization on its physical stability and release profile using Franz diffusion cells.

### MATERIALS AND METHODS

#### Materials

Ibuprofen has been donated by Medifar (Amadora, Portugal). Polysorbate 80 (Tween<sup>®</sup>80) was obtained from Uniqema (Everberg, Belgium). Trehalose, sucrose, and glucose were purchased from Merck S.A. (Lisboa, Portugal). Phosphate buffered saline (pH 7.4), and sorbitan

<sup>1</sup>University of Tiradentes (Unit), Biotechnological Postgraduate Program. Av. Murilo Dantas, 300, 49010–390 Aracaju, Brazil.

<sup>2</sup>Institute of Technology and Research (ITP), Nanomedicine and Nanotechnology Laboratory (LNMed), Av. Murilo Dantas, 300, 49010–390 Aracaju, Brazil.

<sup>3</sup>Tiradentes Institute, 150 Mt Vernon St, Dorchester, MA 02125, USA.

<sup>4</sup>Faculty of Pharmacy, University of Coimbra (FFUC), Pólo das Ciências da Saúde, Azinhaga de Santa Comba, 3000–548 Coimbra, Portugal –Department of Pharmaceutical Technology, Faculty of Pharmacy, University of Coimbra (FFUC), Pólo das Ciências da Saúde, Azinhaga de Santa Comba, 3000–548 Coimbra, Portugal.

<sup>5</sup>Department of Biology and Environment, University of Trás-os-Montes e Alto Douro, UTAD, Quinta de Prados, P–5001–801 Vila Real, Portugal.

<sup>6</sup>CEB – Centre of Biological Engineering, University of Minho, Campus de Gualtar 4710–057 Braga, Portugal.

Received 05 June 2020 Accepted 21 August 2020; Available online 25 September 2020.

DOI: <https://doi.org/10.52466/ijamb.v3i2.37>

monooleate (Span®80) were purchased from Sigma–Aldrich (Steinheim, Germany). Cellulose membrane with an average pore size of 0.22 µm was obtained from Millipore® HA. Ultra–purified water was obtained from the Milli®Q Plus system.

### Nanocrystal production by melt emulsification

The melt–emulsification methodology was used to produce nanocrystals as previously described<sup>(3,4)</sup>. Ibuprofen 0.25% (w/v) was added to the aqueous surfactant solution composed of Tween® 80 (1.0%, w/v) and Span® 80 (0.5%, w/v) heated at 80°C. The suspension was homogenized by high shear homogenization in Ultra Turrax® (T25, IKA) for 10 minutes to obtain a coarse emulsion. The obtained emulsion was poured into a high–pressure homogenizer (EmulsiFlex®–C3, Avastin) and homogenized at 1000 bar for 20 minutes in the continuous mode under heating at 80°C. Finally, the hot formulation was then cooled down using an ice bath for approximately 20 minutes.

### Lyophilization

Nanocrystals were freeze–dried using three different cryoprotectants, trehalose (T), glucose (G) and sucrose (S). Nanocrystal dispersions were diluted with aqueous cryoprotectant solutions at 4:1, 3:1 and 2:1 (v/v) prior to freeze–drying, and frozen to –80°C in a freezer immediately before freeze–drying in a Gamma 2–20 freeze dryer (Christ, Osterode a.H., Germany) operating at –25°/0.025 mBar for a period of 24 h (for the main freezing) and over 6 h drying<sup>(12)</sup>. The lyophilized samples were then dispersed in double distilled water and filtered by a 0.22 µm pore membrane and reanalyzed for their mean particle size and PI<sup>(13)</sup>.

### Particle size analysis

The mean particle size (z–Ave) and polydispersity index (PI) were measured by dynamic light scattering (DLS), in freshly prepared nanocrystals, using a particle size analyzer (DelsaNano C Submicron, Beckman Coulter Delsa, Krefeld, Germany). The measurements were run in triplicate, recording 10 readings per run<sup>(14)</sup>.

### In vitro release profile

The release profile of ibuprofen from the obtained nanocrystals (before and after freeze–drying) was studied using vertical Franz diffusion cells (n = 3 cells/sample). In each cell, a cellulose Millipore HA membrane with an average pore size of 0.22 µm was used previously soaked for at least 1 hour with receptor fluid (phosphate–buffered saline (PBS) at pH 7.4). At pre–determined time intervals, 200 µL of the samples were collected using a syringe, and the same volume was replaced with PBS. The samples were analyzed by ultraviolet (UV) assay at 264 nm, in a Synergy™ HT Multi–Mode Microplate Reader. PBS at pH 7.4 was used as receptor medium and maintained at 37°C during the tests (3).

### Results and discussion

Ibuprofen (IBU), a name derived from isobutyl propanoic phenolic acid, is non–steroidal anti–inflammatory drug with proven effectiveness for treating pain, fever, and inflammation. IBU is one of the most commonly used non–steroidal anti–inflammatory drugs (NSAIDs). It is the weakest of the NSAIDs but reversely has a prominent analgesic and antipyretic actions. Its mechanism of action concerns a non–selective inhibition of cyclooxygenase type 1 (COX–1) and cyclooxygenase type 2 (COX–2). Its side effects are mainly due to the oral intake of this drug which produces an inhibitory action on cyclooxygenases, which are related with prostaglandins' synthesis. Prostaglandins are associated with the production of pain, inflammation and fever.

Extensive research has been put forward with the aim to improve the use of IBU in topical application to overcome its common side effects and low bioavailability<sup>(15,16)</sup>. Our group has described nanocrystal suspensions of IBU stabilized with a combination of surfactants and melt–emulsification processes<sup>(3,4)</sup> using different types of surfactants. In this work, we highlight the combination of Tween® 80/Span® 80 to stabilize IBU nanocrystals in aqueous dispersion. Both surfactants are widely used in pharmaceutical formulation. These surfactants are generally recognized as safe (GRAS) as non–toxic, non–irritating and of low cost. The method production was based on homogenization because it is easily be performed on a small and large scale concerning industrial pharmaceutical.

The produced IBU–NCs were analyzed by particle size and Pdl. The fresh sample showed a particle size and Pdl of 159.4 ± 3.265 nm and 0.24 ± 0.007, respectively. The size of NCs formulation is dependent on the composition/concentration of formulation and method of production. Generally, the high homogenization produces small droplets due to high pressure and fast cooling. Particle size is important for skin permeation, and the ideal size for penetration of the skin is under 700 nm<sup>(17)</sup>. Also, Lademann et al.<sup>(18)</sup>, Adib et al.<sup>(19)</sup> suggested that a particle size between 300–600 nm promote drug penetration significantly more in–depth into the skin layer. The Pdl is a parameter for defining the particle size distribution. Samples with a wide particle size distribution usually have a polydispersion index > 0.7<sup>(20)</sup>. Pdl of 0.4 shows a heterogeneous particle size distribution, and the presence of agglomerates in the dispersion<sup>(21)</sup>. In this study, the obtained Pdl is attributed to the

rearrangements of polysorbate and sorbitan monooleate chains on the surface of nanocrystals. The obtained Pdl value was considered low, and a homogeneous sample was produced.

The choice of cryoprotectant and its concentration is essential for obtaining a stable and reproducible product. The absence of cryoprotecting agents in the drying stage can occasionally produce NCs with sticky and thick components, and if reconstituted, there is the production of aggregates. Thus, the correct choice will allow easy redispersion of the freeze-dried formulation<sup>(22)</sup>. As shown in Table I, the lyophilization slightly increased the mean particle size of IBU-NCs measured after their reconstitution with double distilled water, however remaining within the nanometer range. A low Pdl could be seen in particular for the NCs:Glucose (3:1) combination. All IBU-NCs powders were of white, fine and uniform texture. The NCs:Trehalose (2:1), NCs:Glucose (3:1) and NCs:Sucrose (4:1) for further studies.

In vitro release profile of ibuprofen from non-lyophilized nanocrystals has been compared with the profiles of the resuspended nanocrystals freeze-dried with different cryoprotectant, over a period of 24 hours (Figure 1). Selected cryoprotectant was based on the lowest mean particle size and polydispersity index, namely NCs: Trehalose (2:1) of  $170.6 \pm 3.880$  nm (PI  $0.417 \pm 0.050$ ), NCs:Glucose (3:1) of  $275.3 \pm 8.351$  nm (PI  $0.144 \pm 0.021$ ), and NCs:Sucrose (4:1) of  $223.3 \pm 10.35$  nm (PI  $0.402 \pm 0.016$ ), covered by a combination of Tween<sup>®</sup> 80 and Span<sup>®</sup> 80.

As shown in Figure 1, the release profile allowed the identification of a burst release occurring within the first 10 min, during which approximately 50% of the drug was immediately released in all lyophilized samples. Within the first 6 h, NCs:Trehalose (2:1), NCs:Glucose (3:1) and NCs:Sucrose (4:1) released about 70%, 65% and 50% of the drug, respectively. The slower drug release observed among the samples can be attributed to the interaction between the surfactants, cryoprotection and the drug. Within 24 h, all resuspended freeze-dried samples released almost 100% of the drug. A delayed release was observed for the non-lyophilized IBU nanocrystals; within the first 30 mins only 30% of the drug has been quantified in the receptor medium in contrast to ca. 55% of the lyophilized formulations. The higher hydration capacity of these latter justifies the higher cumulative IBU released over the course of the experiment.

According Patel et al., 2018<sup>(23)</sup> the release profile observed in this study is typical of nanocrystal formulations. Nanocrystal interact with skin overcoming the barrier and reaching cellular level and increase the saturation solubility and concentration gradient easing passive penetration through the skin. Also, this technology is widely used in cosmetics and ointments and emulsions to improve improve formulation stability, tolerance and obtain more product esthetically. Similar results were obtained by rutin<sup>(24)</sup>, flavonoids<sup>(25)</sup> and quercetin<sup>(26)</sup>.

**Table I.** Mean particle size (z-AVE) and polydispersity index (Pdl) of ibuprofen nanocrystals before (non-lyophilized) and after lyophilization. Nanocrystals were re-suspended in ultra-purified water prior to measurements.

<b>Samples</b>	<b>z-AVE (nm)</b>	<b>Pdl</b>
<b>NCs (non-lyophilized)</b>	<b><math>159.4 \pm 3.265</math></b>	<b><math>0.24 \pm 0.007</math></b>
NCs:Trehalose (4:1)	$188.2 \pm 3.696$	$0.409 \pm 0.01$
NCs:Trehalose (3:1)	$234.2 \pm 5.217$	$0.440 \pm 0.024$
<b>NCs:Trehalose (2:1)</b>	<b><math>170.6 \pm 3.880</math></b>	<b><math>0.417 \pm 0.050</math></b>
NCs:Glucose (4:1)	$306.8 \pm 5.488$	$0.751 \pm 0.012$
<b>NCs:Glucose (3:1)</b>	<b><math>275.3 \pm 8.351</math></b>	<b><math>0.144 \pm 0.021</math></b>
NCs:Glucose (2:1)	$376.4 \pm 3.972$	$0.552 \pm 0.026$
<b>NCs:Sucrose (4:1)</b>	<b><math>223.3 \pm 10.35</math></b>	<b><math>0.402 \pm 0.016</math></b>
NCs:Sucrose (3:1)	$223.9 \pm 13.33$	$0.489 \pm 0.030$
NCs:Sucrose (2:1)	$347.6 \pm 5.147$	$0.665 \pm 0.040$

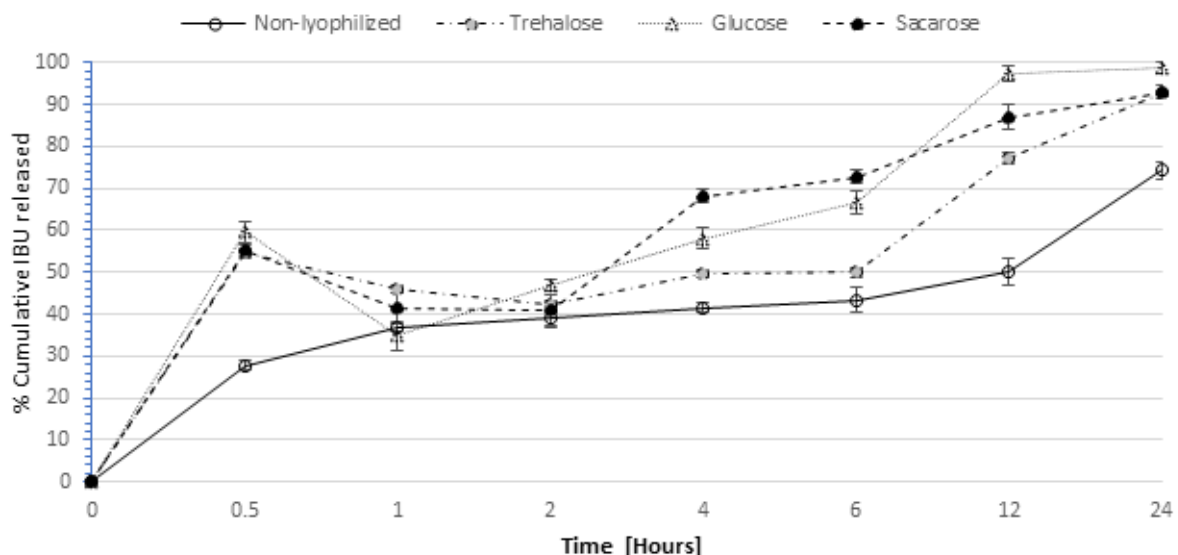


**Figure 1.** *In vitro* IBU release profiles of nanocrystals dispersions before freeze–drying (non–lyophilized) and after freeze–drying with trehalose (2:1), Glucose (4:1) and Sucrose (3:1). Data were recorded at pre–defined time points for a period of 24 h.

### Conclusions

The advantages of IBU nanocrystals as delivery system is attributed to the possibility to enhance the drug solubility and stability. Nanocrystals can be lyophilized to enhance their stability retaining their capacity to modify the release profile. The type and concentration of the cryoprotectant were found to influence the mean particle size, polydispersity index and release profile.

### Acknowledgments

This work was financed through the projects M–ERA–NET/0004/2015 and UIDB/04469/2020, from the Portuguese Science and Technology Foundation, Ministry of Science and Education (FCT/MEC) from national funds, and co–financed by FEDER, under the Partnership Agreement PT2020. Also, this research was funded by Coordenação Aperfeiçoamento de Pessoal de Nivel Superior (CAPES), Fundação de Amparo à Pesquisa do Estado de Sergipe (FAPITEC), and Conselho Nacional de Desenvolvimento Científico e Tecnológico.

### REFERENCES

- [1]. Jahnvi K, Reddy PP, Vasudha B, Narender B. Non–steroidal anti–inflammatory drugs: an overview. *J Drug Deliv* 2019;9(1–s):442–8.
- [2]. Moilanen E, Vuolteenaho K. Nonsteroidal Anti–inflammatory Drugs. *Nijkamp and Parnham's Principles of Immunopharmacology*: Springer; 2019. p. 689–707.
- [3]. Fernandes A, Dias–Ferreira J, Cabral C, Garcia M, Souto E. Release kinetics and cell viability of ibuprofen nanocrystals produced by melt–emulsification. *Colloids and Surfaces B: Biointerfaces* 1. 2018;166:24–8.
- [4]. Fernandes A, Ferreira N, Fangueiro J, Santos A, Veiga F, Cabral C, et al. Ibuprofen nanocrystals developed by 22 factorial design experiment: a new approach for poorly water–soluble drugs. *Saudi Pharm J* 2017;25(8):1117–24.
- [5]. Fernandes AR, Dias–Ferreira J, Ferreira–da–Silva C, Severino P, Martins–Gomes C, Silva AM, et al. Drug nanocrystals: Present, past and future. *Applications of Nanocomposite Materials in Drug Delivery*: Elsevier; 2018. p. 239–53.
- [6]. Hofmann M, Thieringer F, Nguyen MA, Månsson W, Galle PR, Langguth P. A novel technique for intraduodenal administration of drug suspensions/solutions with concurrent pH monitoring applied to ibuprofen formulations. *Eur J Pharm Biopharm.* 2019;136:192–202.

- [7]. Alves TFR, Barros CT, Baldo D, Amaral VA, Sever M, Santos C, et al. Preparation, Characterization and ex vivo Intestinal Permeability Studies of Ibuprofen Solid Dispersion. *J Dispers Sci Technol*. 2019;40(4):546–54.
- [8]. Fangueiro JF, Marques IR, Severino P, Santana MHA, Souto EB. Desenvolvimento, produção e caracterização de nanocristais de fármacos pouco solúveis. *Química Nova*. 2012.
- [9]. Fangueiro JF, Marques IR, Severino P, Santana MHA, Souto EB. Development, production and characterization of nanocrystals of poorly soluble drugs. *Química Nova*. 2012;35(9):1848–53.
- [10]. Teeranachaideekul V, Junyaprasert VB, Souto EB, Muller RH. Development of ascorbyl palmitate nanocrystals applying the nanosuspension technology. *Int J Pharm*. 2008;354(1–2):227–34.
- [11]. Muller RH, Runge S, Ravelli V, Mehnert W, Thunemann AF, Souto EB. Oral bioavailability of cyclosporine: solid lipid nanoparticles (SLN) versus drug nanocrystals. *Int J Pharm*. 2006;317(1):82–9.
- [12]. Doktorovova S, Shegokar R, Fernandes L, Martins–Lopes P, Silva AM, Muller RH, et al. Trehalose is not a universal solution for solid lipid nanoparticles freeze–drying. *Pharmaceutical development and technology*. 2014;19(8):922–9.
- [13]. Gol D, Thakkar S, Misra M. Nanocrystal–based drug delivery system of risperidone: lyophilization and characterization. *Drug Dev Ind Pharm*. 2018;44(9):1458–66.
- [14]. Cavendish M, Nalone L, Barbosa T, Barbosa R, Costa S, Nunes R, et al. Study of pre–formulation and development of solid lipid nanoparticles containing perillyl alcohol. *JTAC*. 2019:1–8.
- [15]. Salim N, García–Celma MJ, Escribano E, Nolla J, Llinàs M, Basri M, et al. Formation of Nanoemulsion Containing Ibuprofen by PIC Method for Topical Delivery. *Mater Today Proc*. 2018;5:S172–S9.
- [16]. Bagde A, Patel K, Kutlehria S, Chowdhury N, Singh M. Formulation of topical ibuprofen solid lipid nanoparticle (SLN) gel using hot melt extrusion technique (HME) and determining its anti–inflammatory strength. *Drug Deliv Transl Res*. 2019:1–12.
- [17]. Alvarez–Román R, Naik A, Kalia Y, Guy RH, Fessi H. Skin penetration and distribution of polymeric nanoparticles. *J Control Release*. 2004;99(1):53–62.
- [18]. Lademann J, Richter H, Meinke MC, Lange–Asschenfeldt B, Antoniou C, Mak WC, et al. Drug delivery with topically applied nanoparticles: science fiction or reality. *Skin Pharmacol Physiol*. 2013;26(4–6):227–33.
- [19]. Adib ZM, Ghanbarzadeh S, Kouhsoltani M, Khosroshahi AY, Hamishehkar H. The effect of particle size on the deposition of solid lipid nanoparticles in different skin layers: A histological study. *Adv Pharm Bull*. 2016;6(1):31.
- [20]. Nidhin M, Indumathy R, Sreeram K, Nair BU. Synthesis of iron oxide nanoparticles of narrow size distribution on polysaccharide templates. *Bull Environ Contam Toxicol* 2008;31(1):93–6.
- [21]. Krause B, Mende M, Pötschke P, Petzold G. Dispersability and particle size distribution of CNTs in an aqueous surfactant dispersion as a function of ultrasonic treatment time. *J Carbon*. 2010;48(10):2746–54.
- [22]. Sharma M, Mehta I. Surface stabilized atorvastatin nanocrystals with improved bioavailability, safety and antihyperlipidemic potential. *Sci Rep*. 2019;9(1):1–11.
- [23]. Patel V, Sharma OP, Mehta T. Nanocrystal: A novel approach to overcome skin barriers for improved topical drug delivery. *Expert opinion on drug delivery*. 2018;15(4):351–68.
- [24]. Pyo SM, Meinke M, Keck CM, Müller RH. Rutin—increased antioxidant activity and skin penetration by nanocrystal technology (smartCrystals). *Cosmetics*. 2016;3(1):9.
- [25]. Gujar K, Wairkar S. Nanocrystal technology for improving therapeutic efficacy of flavonoids. *Phytomedicine*. 2020:153240.
- [26]. Manca ML, Lai F, Pireddu R, Valenti D, Schlich M, Pini E, et al. Impact of nanosizing on dermal delivery and antioxidant activity of quercetin nanocrystals. *Journal of Drug Delivery Science and Technology*. 2020;55:101482.